

The FIMP-WIMP dark matter in the extended singlet scalar model

Pritam Das,^{1,2,*} Mrinal Kumar Das,^{1,†} and Najimuddin Khan^{3,4,‡}

¹*Department of Physics, Tezpur University, Assam-784028, India*

²*Department of Physics, Indian Institute of Technology Guwahati, Assam 781039, India*

³*School of Physical Sciences, Indian Association for the Cultivation of Science 2A & 2B,
Raja S.C. Mullick Road, Kolkata 700032, India*

⁴*School of physics, Institute for Research in Fundamental
Sciences (IPM), P.O.Box 19395-5531, Tehran, Iran.*

Abstract

We explore the simplest viable dark matter model with a real singlet scalar, vector-like singlet and doublet fermions. The Yukawa couplings associated with the fermion sector play a crucial role in getting the current relic density through Freeze-in and Freeze-out mechanism. We discuss the constraints from the recent muon anomalous magnetic moment experimental data and relic density. We also perform the collider analysis for the FIMP dark matter in the context of 14 TeV LHC experiments with the MATHUSLA100/200 detector. Our analysis shows that one can get enough events > 3 for heavy charged fermion track at 14 TeV LHC with an integrated luminosity $\mathcal{L} = 10^6 \text{ fb}^{-1}$.

* prtmdas9@rnd.iitg.ac.in

† mkdas@tezu.ernet.in

‡ najimuddink@ipm.ir

I. INTRODUCTION

The standard model (SM) of particle physics is indeed one of the most successful theories of the last century; however, it still has a few unsolved empirical observations. Among those unsolved questions, strong CP problem, neutrino mass and mixing, matter-antimatter asymmetry, nature of dark matter and dark energy have been considered as shortfalls of the SM. The last few decades have seen an upheaval in astrophysics and cosmology. The Universe is filled with matter and dark matter (DM) and a large amount of dark energy [69]. From the SM model point of view, there is no sufficient candidate left to propose as a dark matter candidate. Therefore, one must go beyond the SM to explain the current dark matter density. The recent LHC Higgs signal strength data [70, 71] also allows us to include additional fields of the new physics beyond the SM.

Now one can get the exact relic density of the dark matter using various theories [69, 72]. Many of the DM genesis theories are based upon the thermal Freeze-out mechanism. In this Freeze-out mechanism, the weakly interacting massive particles (WIMPs) are considered to be in thermal equilibrium in the early universe. When the primordial temperature drops below the mass of the DM, *i.e.*, $T < M_{DM}$, it dilutes away until the annihilation and/or co-annihilation to lighter particles becomes slower than the rate of expansion of the universe; hence, the co-moving DM number density becomes constant. In the literature, we have now seen that most of the single component WIMP dark matter model are tightly constrained by the recent direct detection limits [73]. The low mass region may give the relic density in the right ballpark $\Omega h^2 = 0.1198 \pm 0.0026$ [74]. However, the direct detection limits exclude most of the region [75–78]. Hence, multi-component dark matter models are more appealing at the current scenario [79].

Recently the authors of the Ref. [72], have introduced the idea of the Freeze-in mechanism. The dark matter interacts with the other particle feebly, called Feebly Interacting Massive Particles (FIMPs). Initially, we assume that the dark matter density remains small in the early universe. The idea is that the dark matter particle(s) get populated through the decay and/or annihilation of the other heavy particles in this model. After a certain temperature, the production of the dark matter through all the processes are ended ($T < M_{Mother\ Particles}$), and the co-moving DM number density becomes constant. It is also confirmed that if the same couplings are involved in both the decay and annihilation scattering processes, then the latter case has negligible contribution to DM relic density over the former one [72, 80, 81]. There are two types of Freeze-in mechanisms that have been discussed in the literature. The infra-red (IR) Freeze-in [72, 80, 81] and ultra-violet (UV) Freeze-in [82]. The earlier one based on renormalizable theory and the latter based on theory consists of higher dimension operators in the Lagrangian. The relic density in the UV Freeze-in mechanism depends explicitly on the reheat temperature. It is also noted that the dark DM density depends on the partial decay width (DM production channels only) of the mother particles. The other decay channel may reduce the mother particles density at $T < M_{DM}$

rapidly. However, at $T > M_{DM}$, the reverse processes can compensate the mother particles density from the other bath particles. But the forward DM production channels from the mother particles ($p_{mothers} \rightarrow p_{others} p_{DM}, p_{mothers} \rightarrow p_{DM} p_{DM}$) are very slow due to the smaller coupling strengths, hence the reverse processes ($p_{others} p_{DM} \rightarrow p_{mothers}, p_{DM} p_{DM} \rightarrow p_{mothers}$) cannot take place due to the reasons of coupling strengths as well as the initial density of the produce DM particles. Therefore, the other decay channels of the mother particles will not affect the relic density calculations in the Freeze-in mechanism as the mother particle was thermally equilibrium with the other particles in the early universe [72]. Thus, we have to solve only one Boltzmann equation for the evolution of the DM. In this case, one has to consider the sum of all DM production through the decay and annihilation channels of different mother particles. Suppose the mother particles are not in thermal equilibrium, then we need to solve the evaluation of the mother particles, and at the same time, we have to solve the evaluation for the DM particle [81]. Before or near the Freeze-in temperature, the mother particles' density should go very small so that the decay and annihilation contributions become zero. Hence, to explain the DM density through the IR Freeze-in mechanism, we need a tiny partial decay of the mother particles, *i.e.*, and the coupling strength should be $\mathcal{O}(10^{-9})$. One may ask the question about the naturalness of the theory, the answer itself lies in the Freeze-in mechanism. By default, we need such a small coupling to explain the DM density. In the UV Freeze-in mechanism, one could achieve these similar coupling strengths by adjusting the heavy cut-off scale in the Lagrangian. However, the dynamic reasons for such tiny coupling strengths are beyond the scope of this work.

The lepton flavor violating processes ($\mu \rightarrow e\gamma$) along with the muon and electron anomalous magnetic moment are also a striking indication of BSM. The discrepancy between the measured value and the SM predictions is there [83–85]: $\delta a_\mu = a_\mu^{\text{exp}} - a_\mu^{\text{SM}} = (2.51 \pm 0.59) \times 10^{-9}$ and $\delta a_e = a_e^{\text{exp}} - a_e^{\text{SM}} = -(8.8 \pm 3.6) \times 10^{-13}$. The recent results from Fermilab predicts that the muon anomalous magnetic moment deviates at 4.2σ from the SM prediction [83]. Earlier, it was measured with 3.7σ deviation from the SM prediction at Brookhaven National Laboratory. The muon magnetic moment is more sensitive hadronic and electroweak contributions, as well as BSM physics due to it's large mass, which influences such larger discrepancies between the δa_μ . In the meanwhile, the electron anomalous magnetic moment results doesn't allow much deviation¹ [86]. The discrepancy of the muon magnetic moment can be solved by additional Higgs boson[87, 88] and a light Z' gauge boson associated with an extra $U(1)_{L_\mu-L_\tau}$ symmetry [89], or a light hidden photon [90], imposing discrete symmetries [91]. Apart from these, various models with collider searches have also been discussed in the literature [92–98], where both the anomalies and dark matter were discussed nicely.

The addition of the new fields to the SM is widespread in the literature. The lightest and stable

¹ In this work, we take both the discrepancies as input value to test whether our model can fit those anomalies or not.

particle (at least lifetime of DM should larger than the age of the universe) due to the imposed discrete Z_n -charges ($n \geq 2, integer$), behaves as a viable dark matter candidate [99]. Various study on minimal DM models considering scalar and fermion multiplets are available today [75, 76, 100–103]. In particular, the addition of real singlet scalar, singlet as well as doublet fermion in a minimal model [104, 105], have rich demand in DM study. The mixing of singlet and doublet fermions reduces the coupling to weak gauge bosons and other fermions, yielding the relic density at the right ballpark with allowed direct detection cross-section [106]. However, most models have discussed the Freeze-out mechanism with WIMP dark matter mass 50 GeV – 300 TeV. The dark matter mass above 300 TeV violates the perturbativity bound [107], and the low dark matter mass region is either ruled out by the Higgs signal strength data or direct detection search limits.

In the previous work, [105], it was found that only the singlet scalar WIMP dark matter model with mass less than ~ 550 GeV (except near the Higgs resonance region) are ruled out from recent direct detection limits [73]. We have also found a considerable increment in the WIMP dark matter parameter spaces in the presence of the new Yukawa couplings. One can reduce the Higgs portal coupling κ to avoid the direct detection limits. The additional t, u -channels through the new fermions can increase the dark matter annihilation cross-section to produce the exact relic density. Regarding the collider search studies, we have found that dilepton+ \cancel{E}_T signature can arise from the new fermionic sector and observed at the Large Hadron Collider (LHC). We have performed the collider analysis in the context of 14 TeV LHC experiments with a future integrated luminosity of 3000 fb $^{-1}$ for the final state dilepton+ \cancel{E}_T in detail. The projected exclusion contour reaches up to 1050 – 1380 GeV for 3000 fb $^{-1}$ for a light dark matter $\mathcal{O}(10)$ GeV from searches in the $pp \rightarrow E_1^\pm E_1^\mp, E_1^\pm \rightarrow l^\pm S \rightarrow ll + \cancel{E}_T$ channel. In this study, the SM is extended with a real singlet scalar and singlet and doublet fermion [105] is revisited in the context of the low and high dark matter region.

There have been a rich literature of model studies [95, 108–111], where authors have incorporated the analysis of muon anomalous magnetic moments along with neutrino and dark matter mass models. These studies have also tested the validity of their model parameters and dark matter regions in collider searches. Motivated by these studies, in this minimal setup of our model work, we have identified the new parameter space relevant to low dark matter mass from 10 keV to 6 GeV via the Freeze-in mechanism in this present paper. The WIMP dark matter scenario is revisited keeping the collider constraints from the dilepton+ \cancel{E}_T searches [105]. In this minimal model, both low and high DM mass region are studied, including the allowed region from the latest muon anomalous magnetic moment data [83] from the Fermilab. We also carry out the collider study for the FIMP like scenario in the context of 14 TeV LHC experiments with the MATHUSLA100/200 detector. A charged track can be obtained in this model due to the decay of the heavy charged fermion $E_{1,2}^\pm$ into the SM fermions and dark matter. We find that one can get enough events > 3 at 14 TeV LHC with an integrated luminosity $\mathcal{L} = 10^6$ fb $^{-1}$. Soon, if this type of minimal

model turns out to be the FIMP and/or WIMP dark matter model realized in Nature, our present (including [105]) study could estimate a better parameter space. To the best of our knowledge, a detailed analysis of this model has not been done, which motivating us to study the model.

The rest of the work is organized as follows. We have given the complete model description in section II. The possible constraints from the lepton flavour violation decay and new results on muon magnetic moment are discussed in section III. The dark matter analysis through Freeze-out and Freeze-in mechanism is carried out in detail in section IV. The possible collider searches from the LHC charged tracker detector is analyzed in section VI. Finally, we have conclude our work in section VII.

II. MODEL

The model addressed here, contains (i) a real singlet scalar (S), (ii) a vector-like charged fermion singlet E_S^- and (iii) a vector-like fermion doublet, $F_D = (X_1^0 \ E_D^-)^T$. It is to be noted that these additional fermions are vector-like, and hence, they do not introduce any new anomalies [105, 112, 113]. All the newly added particles are considered odd under discrete Z_2 symmetry ($\Psi \rightarrow -\Psi$), such that these fields do not mix with the SM fields. Hence, the lightest and neutral particle is stable and can be considered as a viable dark matter candidate. The Lagrangian of the model read as [105],

$$\mathcal{L} = \mathcal{L}_{\text{SM}} + \mathcal{L}_S + \mathcal{L}_{\mathcal{F}} + \mathcal{L}_{\text{int}}, \quad (2.1)$$

where,

$$\mathcal{L}_S = \frac{1}{2}|\partial_\mu S|^2 - \frac{1}{2}kS^2\phi^2 - \frac{1}{4}m_S^2S^2 - \frac{\lambda_S}{4!}S^4, \quad (2.2)$$

$$\mathcal{L}_{\mathcal{F}} = \bar{F}_D\gamma^\mu D_\mu F_D + \bar{E}_S\gamma^\mu D_\mu E_S - M_{ND}\bar{F}_D F_D - M_{NS}\bar{E}_S E_S,$$

$$\mathcal{L}_{\text{int}} = -Y_N\bar{F}_D\phi E_S - Y_{fi}\bar{\psi}_{i,L}F_D S - Y'_{fi}\bar{l}_{i,R}E_S S + h.c. \quad (2.3)$$

Here, D_μ stands for the corresponding covariant derivative of the doublet and singlet fermions. The left-handed lepton doublet is denoted by $\psi_{i,L} = (\nu_i, l_i)_L^T$, whereas $l_{i,R}$ indicate the right-handed singlet charged leptons, with $i = e, \mu, \tau$ three generation of leptons. L and R stand for left and right chirality of the fermions. The SM Higgs potential is given by, $V^{SM}(\phi) = -m^2\phi^2 + \lambda\phi^4$, with, $\phi = (G^+, \frac{H+v+iG}{\sqrt{2}})^T$ is the SM Higgs doublet. G 's stand for the Goldstone bosons and $v = 246.221$ GeV being the vacuum expectation value of the Higgs H fields. The mass matrix for these charged fermion fields is given by,

$$\mathcal{M} = \begin{pmatrix} M_{ND} & M_X \\ M_X^\dagger & M_{NS} \end{pmatrix}, \quad (2.4)$$

where, $M_X = \frac{Y_{Nv}}{\sqrt{2}}$. The charged component of the fermion doublet (E_D^\pm) and the singlet charged fermion (E_S^\pm) mix at tree level. The mass eigenstates are obtained by diagonalizing the mass matrix with a rotation of the (E_D^\pm E_S^\pm) basis,

$$\begin{pmatrix} E_1^\pm \\ E_2^\pm \end{pmatrix} = \begin{pmatrix} \cos \beta & \sin \beta \\ -\sin \beta & \cos \beta \end{pmatrix} \begin{pmatrix} E_D^\pm \\ E_S^\pm \end{pmatrix}, \text{ with } \tan 2\beta = \frac{2M_X}{M_{NS} - M_{ND}}. \quad (2.5)$$

Diagonalization of eqn. 2.4 gives the following eigenvalues for the charged leptons ($M_{NS} - M_{ND} \gg M_X$) as,

$$M_{E_1^\pm} = M_{ND} - \frac{2(M_X)^2}{M_{NS} - M_{ND}}, \quad M_{E_2^\pm} = M_{NS} + \frac{2(M_X)^2}{M_{NS} - M_{ND}}.$$

The masses of the neutral fermion scalar fields can be calculated as,

$$M_{X_1^0} = M_{ND}, \quad M_S^2 = \frac{m_S^2 + kv^2}{2} \quad \text{and} \quad M_H^2 = 2\lambda v^2. \quad (2.6)$$

Hence, in this model, neutral fermion can not be the DM candidate as $M_{E_1^\pm} < M_{X_1^0} < M_{E_2^\pm}$. Only the scalar fields S for $M_S < M_{E_1^\pm}$ can behave as a viable DM candidate. We will provide a detailed discussion on the new region of the allowed parameter spaces and the effect of the additional Z_2 -odd fermion in the dark matter section IV.

The parameter space of this model is constrained by various bounds arising from theoretical considerations like absolute vacuum stability and unitarity of the scattering matrix, observation phenomenons like dark matter relic density. The direct search limits at LEP and electroweak precision measurements put severe restrictions on the model. The recent measurements of the Higgs invisible decay width and signal strength at the LHC put additional constraints. The dark matter (DM) requirement saturates the DM relic density all alone restricts the allowed parameter space considerably. These constraints are already discussed in our previous paper [105]. We discuss the lepton flavour violation ($\mu \rightarrow e\gamma$), incorporating the new anomalous magnetic moment result in the next section.

III. LEPTON FLAVOR VIOLATION ($\mu \rightarrow e\gamma$) AND ANOMALOUS MAGNETIC MOMENT

In this model, the LFV couplings (in our model, Y_{fi} and Y'_{fi} with $i = e, \mu, \tau$) and model parameters got severely constraint by the bounds from LFV processes. Hence, it is evident that LFV bounds can mimic other observable like DM parameter spaces (one can go through the WIMP dark matter analysis section, carried out in this work). The observed dark matter abundance is typically obtained for $\kappa = Y_{fi}^{all} = \mathcal{O}(0 - 1)$ through s -channel, t -channel annihilation and the

combination of these two processes (co-annihilation, *i.e.*, mass differences can also play a crucial role). The lepton flavour observable are expected to give stringent constraints on the parameter spaces.

Among the various LFV processes, the radiative muon decay $\Gamma(\mu \rightarrow e\gamma)$ is one of the popular and restrictive one, which in the present model is mediated by charged particles E_1^\pm, E_2^\pm present in the internal lines of the one-loop diagram 1. The corresponding expression for the branching

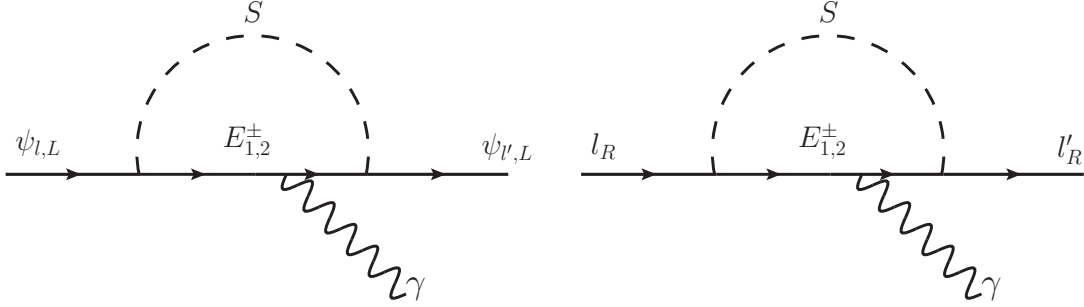


FIG. 1: Muon and electron anomalous magnetic moment and LFV process $\mu \rightarrow e\gamma$ decay diagrams mediated by charged particles E_1^\pm and E_2^\pm .

ratio is given by,

$$\text{BR}(\mu \rightarrow e\gamma) = \frac{3\alpha_{em}}{64\pi G_F^2} \left| A_{f1}^\dagger A_{f2} \frac{F(M_{E_1^\pm}^2/M_S^2)}{M_S^2} + B_{f1}^\dagger B_{f2} \frac{F(M_{E_2^\pm}^2/M_S^2)}{M_S^2} \right|^2, \quad (3.1)$$

where, $F(x) = \frac{x^3 - 6x^2 + 3x + 2 + x \ln(x)}{6(x-1)^4}$. The coupling strengths of the corresponding vertices are $A_{f1} = \cos \beta Y_{f1} + \sin \beta Y'_{f1}$, $A_{f2} = \cos \beta Y_{f2} + \sin \beta Y'_{f2}$, $B_{f1} = \sin \beta Y_{f1} + \cos \beta Y'_{f1}$ and $B_{f2} = \sin \beta Y_{f2} + \cos \beta Y'_{f2}$ respectively. With the most recent experimental bounds for LFV [114], one can get allowed parameters from the lepton flavor violating decay constraints [114] $\text{BR}(\mu \rightarrow e\gamma) < 4.2 \times 10^{-13}$ at 90% CL., for Y_{fj} and $Y'_{fj} < \mathcal{O}(10^{-3})$ with $j = e$ or μ .

Along with the LFV process, the muon anomalous magnetic moment provides new sensitivity for new physics contribution due to the higher level of precision in both theoretical and experimental measurements. The recent measurement of the muon anomalous magnetic moment, $a_\mu = (g - 2)_\mu/2$, at Fermilab shows a discrepancy *w.r.t.* the Standard Model (SM) prediction [83],

$$a_\mu^{FNAL} = 116592040(54) \times 10^{-11}, \quad (3.2)$$

$$a_\mu^{SM} = 116591810(43) \times 10^{-11}, \quad (3.3)$$

and, when it was combined with the previous Brookhaven result [84], $a_\mu^{BNL} = 116592089(63) \times 10^{-11}$ leads to an observed excess of $\delta a_\mu = 251(59) \times 10^{-11}$ at 4.2σ C.L. In the near future experiments at Fermilab, these discrepancies are expected to be clarified with more precise data. The electron

anomalous magnetic moment sensitivity is [83–85]: $\delta a_e = a_e^{\text{exp}} - a_e^{\text{SM}} = -(8.8 \pm 3.6) \times 10^{-13}$. It is negative and one need a very sensitive parameters to solve the electron as well as muon anomalous magnetic moment simultaneously. In our model, with the vector-like fermions in hand, the new contribution to anomalous magnetic moment can be written as [115, 116],

$$\begin{aligned} \delta a_i = & \frac{\text{Re}[A_{f_i}^2]m_l^2}{8\pi^2} \int_0^1 \frac{x(1-x)^2}{(x-x^2)m_l^2 + (x-1)M_{E_1^\pm}^2 - xM_S^2} dx \\ & + \frac{\text{Re}[B_{f_i}^2]m_l^2}{8\pi^2} \int_0^1 \frac{x(1-x)^2}{(x-x^2)m_l^2 + (x-1)M_{E_2^\pm}^2 - xM_S^2} dx, \end{aligned} \quad (3.4)$$

where $i = e, \mu, \tau$. As we can see directly from equation (3.4), the contribution to δa_i depends on the masses ($m_{E_{1,2}^\pm}, M_S$), Yukawa couplings (Y_{f_i} and Y'_{f_i}) and the mixing angle (β). Depending on the new Yukawa couplings Y_{f_i} and Y'_{f_i} , the loop diagram simultaneously contributes to the electron as well as muon anomalous magnetic moment. For simplicity, let us assume all the Y'_{f_i} couplings are negligibly small. We find that, a very large Yukawa couplings ($Y_{f_i} > 4\pi$) are required to explain the present lepton anomalous magnetic moment data. For example, one can get $\delta a_\mu = 2.51 \times 10^{-11}$ for $Y_{f_2} = 29.32$, $M_S = 1000$ GeV, $M_{E_1^\pm} = 1500$ GeV and $M_{E_2^\pm} = 3000$ GeV. This choice of couplings and masses violate the LFV as well as perturbative limits. If we assume non-zero $Y_{f_2} = Y'_{f_2}$, then we also need $Y_{f_2} \sim \mathcal{O}(20)$ to get $\delta a_\mu = 2.51 \times 10^{-11}$. Similarly, we also need a very large $Y_{f_1} = Y'_{f_1}$ to get electron anomalous magnetic moment. On the contrary, these large couplings are not healthy for this model as it will render a large negative potential (become unbounded from below) towards the singlet as well as the Higgs scalar fields due to radiative corrections². To work out this model smoothly, we always kept Y_{f_2} and $Y'_{f_2} < \mathcal{O}(10^{-3})$. It is to be noted, the regions allow by LFV data are also allowed by these anomalous magnetic moment data. In the next section, we discuss the dark matter analysis and bound coming from the relic density.

IV. DARK MATTER

As pointed out in the previous section, the viable DM candidate in this model is the lightest Z_2 -odd singlet scalar S . Here, the dark matter can give exact relic density through the Freeze-out mechanism and/or Freeze-in mechanism, depending on the choice of parameter spaces. Suppose the dark matter is in thermal equilibrium in the early universe; in this case, the dark matter can annihilate to the SM particles when $T > M_{DM}$, where T is the temperature of the universe. It Freezes out for $T < M_{DM}$, and depending on the parameter spaces it could give the exact relic density. However, if it is not in thermal equilibrium in the early Universe, it could produce from some mother particles and give correct relic density through the Freeze-in mechanism. Dark matter

² The detailed analysis with radiative corrections is beyond scope of this work

resulting from a decay or annihilation of various mother particles, is in thermal equilibrium at early universe. This condition is given by,

$$\frac{\Gamma}{H(T)} \geq 1, \quad (4.1)$$

where, Γ is the relevant decay width and $H(T)$ is the Hubble parameter given by [72, 81, 117]

$$H(T) = \left(g^* \frac{\pi^2}{90} \frac{T^4}{M_{\text{Pl}}^2} \right)^{1/2}, \quad (4.2)$$

where, $M_{\text{Pl}} = 2.4 \times 10^{18}$ GeV is the reduced Planck mass and T is the temperature (1 GeV = 1.16×10^{13} Kelvin). If the production of mother particles occur mainly from the annihilation of other particles in the thermal bath, Γ will be replaced by [72, 81, 117]

$$\Gamma = n_{eq} \langle \sigma v \rangle, \quad (4.3)$$

where, n_{eq} is their equilibrium number density and is given by [117]

$$n_{eq} = \begin{cases} g^* \left(\frac{mT}{2\pi} \right)^{3/2} e^{-m/T}, & \text{for non-relativistic states } T \ll M \\ \frac{\zeta_3}{\pi^2} g^* T^3, & \text{for relativistic boson states } T \gg M \\ \frac{3}{4} \frac{\zeta_3}{\pi^2} g^* T^3, & \text{for relativistic fermion states } T \gg M \end{cases} \quad (4.4)$$

where, the Riemann zeta function has the value $\zeta_3 = 1.2$ and g^* is the effective degrees of freedom in this framework. Here, $\langle \sigma v \rangle$ is the thermally averaged annihilation cross-section of the particles in the thermal bath and can be expressed as [117, 118]

$$\langle \sigma_{xx} v \rangle = \frac{2\pi^2 T \int_{4m^2}^{\infty} ds \sqrt{s} (s - 4m^2) K_1\left(\frac{\sqrt{s}}{T}\right) \sigma_{xx}}{(4\pi m^2 T K_2\left(\frac{m}{T}\right))^2}, \quad (4.5)$$

where, $K_{1,2}$ is the modified Bessel function of functions of order 1 and 2 respectively. The DM production through annihilation depends upon the Higgs portal couplings κ through s - and cross-channels (one can reverse the Figs. 2-(a), 2-(b) and 2-(c)) and the new Yukawa coupling Y_{fi} through t -channel (Figs. 2-(d)). Earlier we have checked [105] that for $\kappa, Y_{fi} \sim \mathcal{O}(0.001)$ with DM mass $\sim \mathcal{O}(\text{GeV})$, the dark matter is in thermal equilibrium at early Universe, *i.e.*, $\frac{n_{eq} \langle \sigma_{xx} v \rangle}{H(T)} \gg 1$. These dark matter mass region give the exact relic density via the Freeze-out mechanism.

In this work, we find that the non-thermally produced singlet scalar can also serve as a viable dark matter candidate at $\mathcal{O}(1)$ GeV (depends on the parameters κ, Y_{fi} and β) satisfying the dark matter relic density in the right ballpark. Those light dark matter can interact with other particles very feebly. For such very weakly interacting particles, called feebly interacting massive particles

or FIMPs, one can invoke the non-thermal dynamics, so-called the Freeze-in mechanism. This mechanism needs weak interactions, which could be one reason to have a tiny fine-tuned coupling in this model. In this model, we find that the shallow dark matter mass region $\mathcal{O}(1)$ keV-MeV could also give the exact relic density in the right ballpark.

We will discuss both the dark matter regions coming from the Freeze-out and Freeze-in mechanism in the following two subsections keeping eye on all the constraints. We want to refer to our previous paper [105] for the detailed constraints arising from various theoretical and experimental point of view.

A. WIMP dark matter

The lightest Z_2 -odd singlet scalar S plays the role of viable WIMP dark matter candidate for the choice of region of the parameter spaces with mass $\mathcal{O}(100)$ GeV and annihilation coupling strength $\mathcal{O}(0.1)$ [105]. In our WIMP dark matter study, we use `FeynRules` [119] to get the input codes for `micrOMEGAs` [120] and compute the relic density of the scalar DM. We also verified the results using `SARAH-4.14.3` [121] including `SPheno-4.0.3` [122] mass spectrum in `micrOMEGAs` and get the same relic density of the scalar DM. The Higgs portal couplings κ controls the DM production and/or annihilation through s - and cross-channels (see figs. 2-(a), 2-(b) and 2-(c)). The Yukawa couplings associate with the singlet scalar (Y_{fi} and Y'_{fi}) and the charged fermions (Y_N) also have significant influences [105] in the WIMP DM parameter space. Depending on the Yukawa couplings (Y_{fi} and Y'_{fi}), DM can annihilate via t - and u -channels (see fig. 2-(d)) in our model. The relevant vertices for the dark matter annihilation and/or co-annihilation are given by:

$$\begin{aligned}
g_{HSS} &= |\kappa v|, \quad g_{HHSS} = |\kappa|, \\
g_{SiE_1^\pm} &= A_{fi} = |(\cos \beta Y_{fi} + \sin \beta Y'_{fi})|, \\
g_{SiE_2^\pm} &= B_{fi} = |(\sin \beta Y_{fi} + \cos \beta Y'_{fi})|, \\
g_{S\nu_i X_1^0} &= C_{fi} = |Y_{fi}|, \quad \text{with } i = e, \mu, \tau.
\end{aligned} \tag{4.6}$$

The interference between the s -channel, cross-channel and t, u -channels played a crucial role to achieve the correct DM density. The co-annihilation channels (e.g., see Fig. 3) also have an essential role in getting a viable region of allowed dark matter parameter space. The contributions from the S mediate co-annihilation t, u -channel diagrams is negligibly small. If the mass difference between the DM and other Z_2 -odd particles are within 2%–10%, it is expected that co-annihilation will dominate over DM self-annihilation [123]. We find a huge suppression to the relic density due to large co-annihilation for $M_{E_{1,2}^\pm, X_1^0} - M_S \approx 50$ GeV. Hence most of the higher mass region are ruled out due to the under abundance of a single component dark matter. It is to be noted that the Sommerfeld enhancement [124] do not play any role to enhance the current dark matter

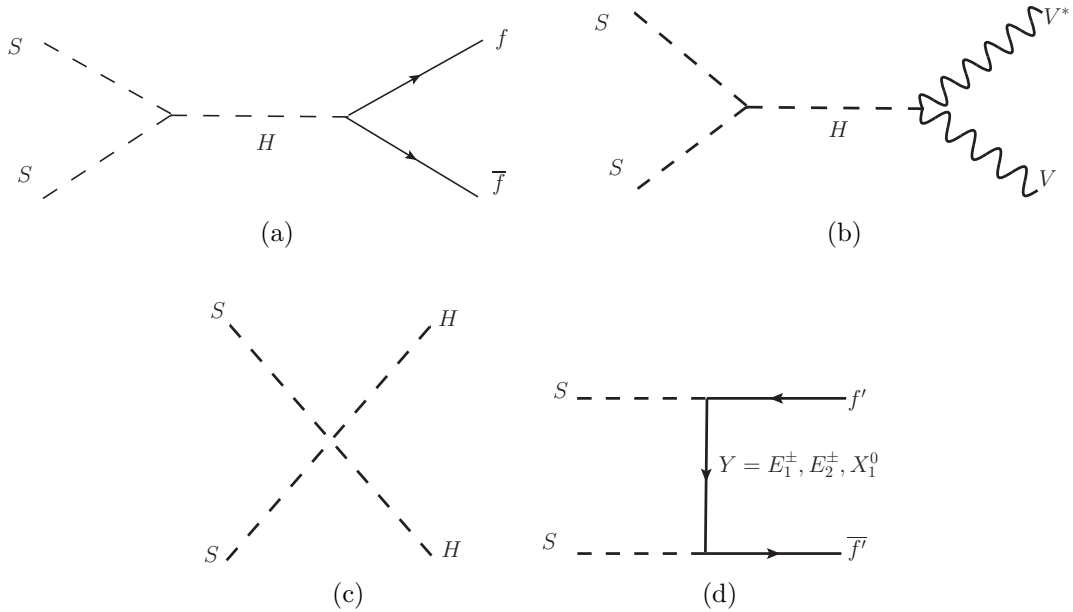


FIG. 2: The DM annihilation diagrams give the relic density. V stands for gauge bosons W, Z ; f' represents the SM leptons and f are SM leptons and quarks.

phenomenology due to $M_{E_{1,2}^\pm} > M_{DM}$.

We already have seen that dilepton+ \cancel{E}_T signature can arise from the new fermionic sector through $pp \rightarrow E_1^\pm E_1^\mp, E_1^\pm \rightarrow l^\pm S \rightarrow ll + \cancel{E}_T$ channel. The charged fermion may observe at the Large Hadron Collider (LHC) with high luminosity. We have already done such analysis in our previous work [105] in the context of 14 TeV LHC experiments with a future integrated luminosity of 3000 fb^{-1} . By performing a detailed cut based collider analysis, we have seen that a large region of the parameter spaces can be probed/excluded by the LHC experiments. The projected exclusion contour have reached up to $1050 - 1380 \text{ GeV}$ for 3000 fb^{-1} for a light dark matter $\mathcal{O}(10) \text{ GeV}$ from searches in the $pp \rightarrow E_1^\pm E_1^\mp, E_1^\pm \rightarrow l^\pm S \rightarrow ll + \cancel{E}_T$ channel. Hence, in this analysis, we keep fixed the mass parameters $M_{E_1^\pm} = 1500 \text{ GeV}$ and $M_{E_2^\pm} = 3000 \text{ GeV}$. For simplicity, we consider the effect from the interaction term $-Y'_{fi} \bar{l}_{i,R} E_S S$ (see eqn. 2.3) to be zero, with $Y'_{fi} = 0$. We will discuss the effect at the end of the WIMP dark matter section. We also assume $Y_{f1} = Y_{f3} = Y_f$ with $Y_{f2} = 0.001$ ³ to avoid flavor violating decays and fixed mixing angle as $\cos \beta = 0.995$. This small mixing angle (β) diluted the contribution from the second charged fermion E_2^\pm . We now scan a prominent region for the DM mass in this work, Higgs portal coupling κ and new Yukawa

³ In general, large Yukawa coupling are also allowed from the relic density. One can also get similar results for the choice of $Y_{f2} = Y_{f3} = Y_f$ and $Y_{f1} = 0.001$ or $Y_{f2} = Y_f$ with $Y_{f1} = Y_{f3} = 0.001$. For different choice of couplings, Fig. 4 (left) remains almost identical; however, the right one gets modified due to having only one dominant contribution from the diagram with the second Yukawa coupling.

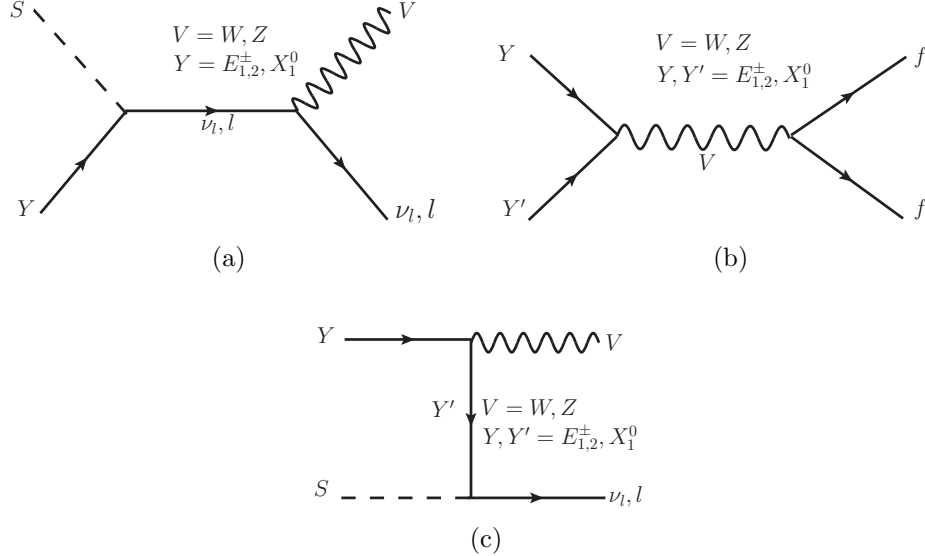


FIG. 3: The co-annihilation and annihilation diagrams of the DM and the other Z_2 -odd fermion fields. f are SM leptons and quarks.

coupling Y_f . The dark matter mass M_{DM} have been scanned from ~ 5 GeV to 1500 GeV with a step size of 5 GeV while Higgs portal coupling changes from -0.6 to 0.6 with step size 0.001 and new Yukawa coupling from -0.5 to 0.5 with step 0.001.

For $\Delta M^{\pm,0} < 0.1M_{DM}$ [123] ($\Delta M^{\pm} = M_{E_1^{\pm}} - M_{DM}$ and $\Delta M^0 = M_N - M_{DM}$), the co-annihilation channels (Fig. 3⁴) play an important role in the dark matter density calculation⁵. It is noted that the co-annihilation effects are completely absent here as $\Delta M^{\pm,0} > 0.1M_{DM}$. We display the allowed parameters $\kappa - M_{DM}$ plane in Fig. 4(left). In the shallow mass region (below $M_H/2$), t, u -channel annihilation processes play a key role in giving rise to correct relic bounds. Those regions are also allowed by Higgs decay width and direct detection bounds. $SS \rightarrow \nu\nu$ are the main dominant channels in this region. In the low DM mass region, annihilation via s -channel, cross-channel and other co-annihilation processes are negligibly small. The Higgs portal coupling is kept very small ($\kappa \sim 0$) to avoid the Higgs signal strength constraints. On the other hand, all the processes, depending on the parameters in the high mass region, are important to provide the exact relic density. The above and below region correspond to Higgs portal coupling $|\kappa| \gtrsim \frac{M_{DM}}{3324.92 \text{ GeV}}$ of 4(left) are strictly ruled out from the direct detection data.

In the absence of new fermion interaction ($Y_f = 0$), DM-mass region in between 70 GeV to 450

⁴ The DM does not participate in diagram 3(b), but this diagram plays an essential role in relic density calculation through co-annihilation processes when $M_Y - M_S \approx (2 - 10)\%$ of M_S .

⁵ There is a missing diagram corresponding to $Sf_V \rightarrow f_{SM}H$, mediated by the t -channel exchange of a f_V , however, due to propagator-vertex suppression, the annihilation channel have very tiny contribution, therefore we have not included that diagram

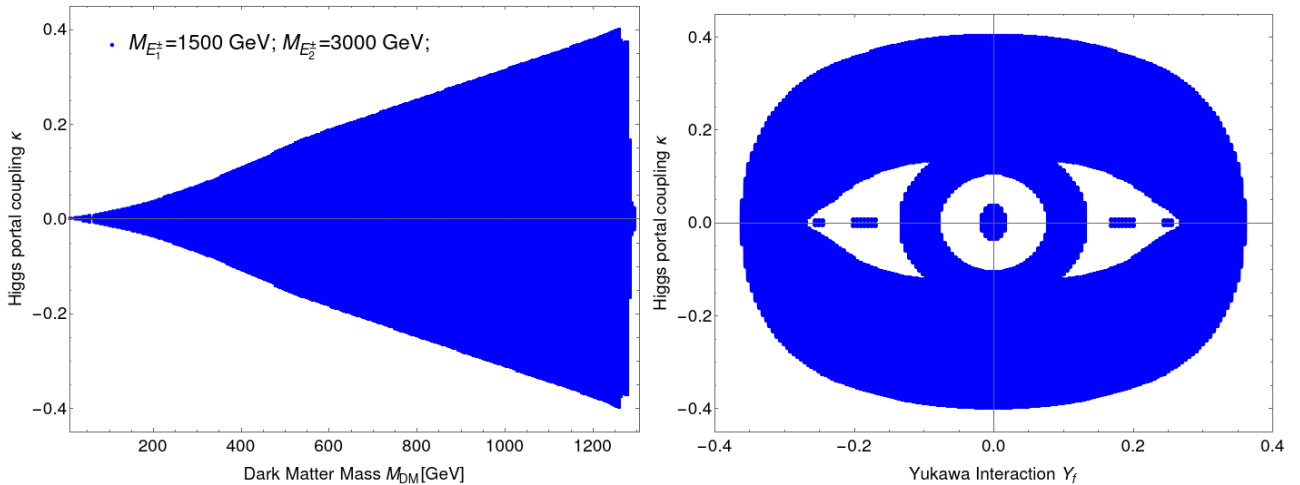


FIG. 4: The blue points indicate the relic density within the 3σ range. These plots are generated by varying the dark matter mass, Higgs portal coupling κ and the new Yukawa coupling Y_f . The empty region in the second plot is mostly disfavoured by the relic density and direct detection constraints. The parameters allowed by relic density are also allowed by the recent LFV [114] $BR(\mu \rightarrow e\gamma) < 4.2 \times 10^{-13}$ at 90% CL, electron as well as muon anomalous magnetic moment $g - 2$ data at Fermilab [83].

GeV is ruled out by the present direct detection cross-section [73]. However, we do not have any DM signature in those experiments at the current date, and by adjusting Higgs portal coupling κ and the new Yukawa coupling Y_f , one can work out this forbidden region. As we increase the viable allowed DM mass, the Higgs portal coupling κ keeps increasing if we neglect the Yukawa coupling Y_f . Similarly, if we choose a small Higgs portal coupling κ , one has to increase the Yukawa coupling Y_f with DM mass to get the relic density at the right ballpark. Variation of these couplings can exceedingly increase dark matter parameter spaces through the combination of s -, t - and u - annihilation and co-annihilation channels.

The $SS \rightarrow VV, HH$ (with $V = W^\pm, Z$) channels keep on dominating in the *mid – high* (500-1000 GeV) DM mass regions. Various allowed benchmark points are shown in Table I. One can see, in the presence of DM annihilation via s -channel and t, u -channels, as most of the regions are giving the correct DM density, which are also allowed by other experimental constraints. For $\kappa \sim 0$, the s -channel annihilation still dominates near Higgs resonance region $\sim \frac{M_H}{2}$. The other mass regions give an overabundance for the same κ and $Y_f \sim 0$. For a small $\kappa \sim 0$, the $t+u$ -channels contribute to get the correct relic density at 3σ C.L., whereas s -channel and *cross*-channel processes dominate for large κ and small Y_f . We have shown the viable region of parameters in the $\kappa - Y_f$ plane in Fig. 4(right). A blue circular eye-like pattern is obtained here. The same data points are also shown in the $\kappa - M_{DM}$ plane of Fig. 4(left). The blue regions are the allowed data points passes by all experimental and theoretical bounds [105] such as stability, perturbativity, unitarity, LHC

Channel	M_{DM} (GeV)	κ	$M_{E_1^\pm}$ (GeV)	Y_f	$\Omega_{DM}h^2$	Percentage
BP-1	10	0.00	1500	0.29	0.115	$\sigma(SS \rightarrow \nu\nu)$ 98% $\sigma(SS \rightarrow ll)$ 2%
BP-2	80	-0.01	1500	0.28	0.1142	$\sigma(SS \rightarrow \nu\nu)$ 98% $\sigma(SS \rightarrow ll)$ 2%
BP-3	270	0.058	1500	0.24	0.113	$\sigma(SS \rightarrow \nu\nu)$ 46% $\sigma(SS \rightarrow W^\pm W^\mp)$ 23% $\sigma(SS \rightarrow HH)$ 13% $\sigma(SS \rightarrow ZZ)$ 11% $\sigma(SS \rightarrow ll)$ 7%
BP-4	760	0.224	1500	0.09	0.1243	$\sigma(SS \rightarrow W^\pm W^\mp)$ 48% $\sigma(SS \rightarrow HH)$ 24% $\sigma(SS \rightarrow ZZ)$ 24% $\sigma(SS \rightarrow ll)$ 3%
BP-5	1000	0.31	1500	0.05	0.114	$\sigma(SS \rightarrow W^\pm W^\mp)$ 49% $\sigma(SS \rightarrow ZZ)$ 24% $\sigma(SS \rightarrow HH)$ 24% $\sigma(SS \rightarrow ll)$ 2%
BP-6	1285	0.372	1500	0.035	0.112	$\sigma(E_1^\pm S \rightarrow W^\pm \nu)$ 45% $\sigma(X_1 S \rightarrow W^\pm l)$ 32% $\sigma(SS \rightarrow \nu\nu)$ 9% $\sigma(SS \rightarrow W^\pm W^\mp)$ 2%

TABLE I: *The benchmark points allowed by all the theoretical and experimental constraints. $\sigma(SS \rightarrow \nu\nu)$ is mainly dominated by the $t + u$ -channel annihilation processes whereas $\sigma(SS \rightarrow YY)$, $Y = W, Z, H, t$ dominated by the $s +$ cross-channel annihilation processes. We consider $Y_{f1} = Y_{f3} = Y_f$ to avoid flavor violating decay processes.*

diphoton signal strength, electroweak precision experiments, lepton flavour violation and lepton anomalous magnetic moments⁶. The empty region violates one of the constraints, such as the relic density of the dark matter, direct detection, and Higgs decay width for the DM mass $< \frac{M_H}{2}$. There is large excluded region for $\kappa, Y_f \sim 0$ compared to the presence of both κ and Y_f . For example, the points $Y_f \approx 0, \kappa \approx 0$ give exact relic density for the dark matters masses near Higgs resonance, i.e., $55 < M_{DM} < 64$ GeV. We get under abundance around $M_{DM} \approx M_h/2 \pm 1$. This can be seen in the left panel of the Fig. 4. The central region of the eye is also dominated mainly by the co-annihilation channels where $\Delta M^{\pm,0} < 0.1M_{DM}$ for high dark matter masses. The following

⁶ We are getting $\delta\alpha_i < 10^{-15}$ (with $i = e, \mu$) hence, lepton anomalous moment bounds are satisfied here. On the contrary, to get exact value of $\delta\alpha_i$, we need very large Yukawa coupling, which is restricted by the perturbativity bounds.

circular empty region is produced under abundance due to a large co-annihilation cross-section for the high dark matter mass. The blue iris-eye region is now allowed for the other masses, where the co-annihilation effects are negligible. Both the side of this iris-eye region is also produced under-abundance due to the effect of additional dark matter annihilation through the s, t and u channel processes for different dark matter masses. The small blue region (both the left and right side) gives the exact relic density for the low dark matter masses $M_{DM} < 100$ GeV through the t and u channel processes. The bigger blue region has all possible effects on the relic density for various dark matter masses. The outer side of the blue region is mostly ruled out from the direct detection data. The low DM mass region was satisfying the current relic density within 3σ C.L., obtained via the t, u -channel processes. The s -channel annihilation processes in the low mass region were considerably absent; hence, very few allowed points for $\kappa \sim 0$ were observed on the right side of Fig. 4. In those scenarios mainly $E_1^\pm E_1^\pm \rightarrow YY$ (with $Y = W^\pm, Z, H$) via t, u -channels and other annihilations and/or co-annihilations dominate and the relic density gets under-abundant for large Y_f and become overabundant for $Y_f = 0$. As we move towards the higher mass regions, both the annihilations and co-annihilations processes start dominating. Please note that, the co-annihilations processes fully dominate in the region where we have $\Delta M^{\pm,0} \ll 0.1M_{DM}$. Hence, large points satisfying the relic density within 3σ C.L. are observed for a wider variety of κ, Y_f and M_{DM} .

It is important to highlight that the small mixing angle (β) and large mass $M_{E_2^\pm} = 3000$ GeV diluted the contribution from the new second charged fermion E_2^\pm . This eigenstate is mostly composed of the $SU(2)$ singlet charged fermion E_S^\pm due to this choice of small mixing angle. One can increase the percentage of E_D^\pm component in the same eigenstate E_2^\pm by decreasing the value of this mixing angle. At the same time the coupling strengths of the t, u -channels vertices $g_{E_1^\pm l \mp S} = \cos \beta Y_{fi}$ and $g_{E_2^\pm l \mp S} = \sin \beta Y_{fi}$ get modified. It influences the annihilation of the dark matter through t, u -channels; hence the relic density will change. For example, one can find the exact relic density allowed by all the other constraints for the dark matter mass $M_{DM} = 270$ GeV (see BP-3 of table I) with Higgs portal coupling $\kappa = 0.058$ and $Y_f = 0.25$ with fixed $\cos \beta = 0.995$ and $M_{E_2^\pm} = 3000$ GeV. In this case, if we change $\cos \beta = 0.6$, then we get an overabundance of the dark matter density $\Omega_{DM} h^2 > 0.15$. To achieve the exact relic density, we need to decrease the value of the mass of the second eigenstate and/or increase the new Yukawa coupling Y_f . For example, by lowering the mass eigenstate of E_2^\pm to $M_{E_2^\pm} = 1510$ GeV and keeping the same $Y_f = 0.24$ or keeping $M_{E_2^\pm} = 3000$ GeV with $Y_f = 0.301$, one can get $\Omega_{DM} h^2 = 0.113$. It is important to note that the left plot of the Fig. 4 will remain almost same for the choice of different mixing angle $\cos \beta$ and fixed $M_{E_2^\pm} = 3000$ GeV as the Higgs portal coupling $|\kappa|$ is constrained from the dark matter direct detection. However, the right plot of Fig. 4 will be modified. One can have larger allowed region in the $Y_f - \kappa$ plane from the relic density and other constraints. The allowed values of new Yukawa coupling can reach up to $Y_f \leq 0.391$ for $\kappa = 0$ and $\cos \beta = 0.6$ in the $Y_f - \kappa$

plane. We show the effect of the mixing angle in Fig. 5 (left) of the t, u -channels contribution in the relic density.

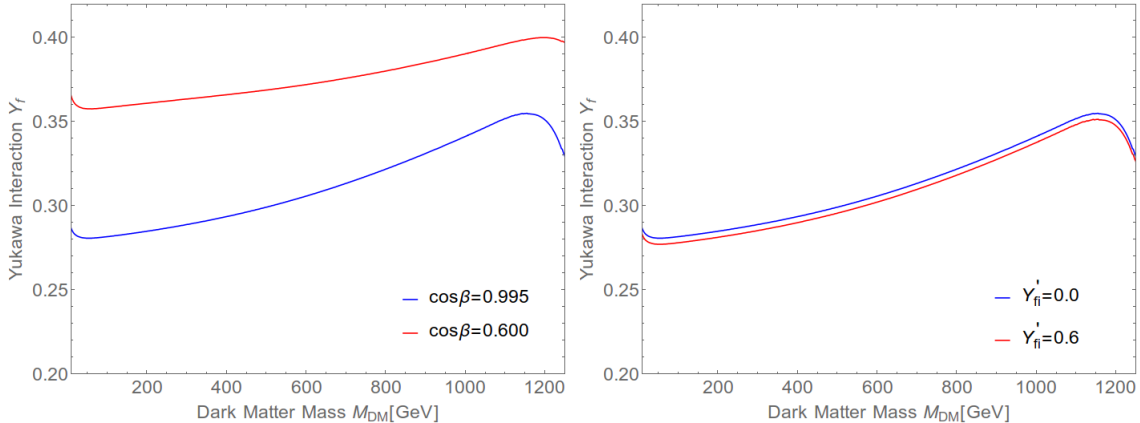


FIG. 5: The blue and red lines indicate the relic density $\Omega_{DM}h^2 = 0.1198$. These plots are generated by varying the dark matter mass and the new Yukawa coupling Y_f for different $\cos\beta$ and Y'_{fi} . The values $Y'_{fi} = 0$ (left panel) and $\cos\beta = 0.995$ (right panel) remain fixed. The masses $M_{E_1^\pm} = 1500$ GeV and $M_{E_2^\pm} = 3000$ GeV and $\kappa = 0$ are same for both cases. These parameters allowed by relic density are also allowed by the recent LFV, electron as well as muon anomalous magnetic moment $g - 2$ data.

One can also consider non-zero Y'_{fi} to get enhancement (for the same sign of Y_{fi}) in the dark matter annihilation as well as co-annihilation into the SM particles, and for $\cos\beta = 0.995$ this enhancement is small. We show the effect in Fig. 5 (right) that, one needs smaller Y_f to get relic density for non-zero Y'_{fi} . The blue and red lines satisfy the relic density $\Omega_{DM}h^2 = 0.1198$. The blue line correspond to $Y'_{fi} = 0$ whereas red line stand for the choice $Y'_{fi} = 0.6$. The Higgs portal coupling $\kappa = 0$, mixing angle $\cos\beta = 0.995$ and masses $M_{E_1^\pm} = 1500$ GeV and $M_{E_2^\pm} = 3000$ are same in both cases.

It is also noteworthy that the non-zero Yukawa coupling Y_{f2} (and $Y_{f1} = Y_{f3} = Y_f$) puts additional contribution to the processes $\Gamma(\mu \rightarrow e\gamma)$. and throughout this analysis, we keep fixed $Y_{f2} = \mathcal{O}(10^{-3})$. The parameters shown in Fig. 4 are all allowed from the most stringent constraints of the flavour violating decay [114] $\text{BR}(\mu \rightarrow e\gamma) < 4.2 \times 10^{-13}$ at 90% CL. We also get negligibly small contributions to the electron as well as muon anomalous magnetic moment for the allowed parameters. These contributions can have positive and/or negative impacts depending upon the choice of parameters. Possibly, with $M_S = 1000$ GeV, $M_{E_1^\pm} = 1500$ GeV and $M_{E_2^\pm} = 3000$ GeV, one needs $Y_{f2} = 29.32$, to reproduce the present experimental data $\delta a_\mu = 2.51 \times 10^{-11}$ [83]. However, this choice of couplings and masses violate the LFV as well as perturbative limits $Y_{fi} > 4\pi$. Hence, the parameters allowed by relic density are also allowed by the recent electron as well as muon anomalous magnetic moment $g - 2$ data at Fermilab [83]. However, the converse is not true in our

model, as the region allowed by electron and/or muon anomalous magnetic moment $g - 2$ data violates the relic density, LFV as well as perturbative bounds.

B. FIMP dark matter

We again want to remind the readers about the FIMPs. The main idea is that the dark matter sector gets populated through decay or annihilation of heavy particles until the number density of the corresponding heavy particle species become Boltzmann-suppressed. We need to solve Boltzmann equations that dictate the final relic abundance for the dark matter candidate S . One can easily calculate the decay width or annihilation of the heavy mother particles from the other particles. The coupling strengths are $\mathcal{O}(1)$, and we get $\Gamma/H \gg 1$ for the mother particles. Hence, all the mother particles (SM particles including heavy fermions) remain in the thermal equilibrium in the early Universe. Therefore we do not need to solve the Boltzmann equation for the evaluation of the mother particles, rather we have only solved the evaluation equation for the dark matter produces from the decay and annihilation of various mother particles.

This model can produce dark matter from the decay of the heavy fermions ($X_{Heavy} = E_1^\pm, E_2^\pm$ and X_1^0) and Higgs. It has already been noticed in the existing literature [72, 80, 81, 125, 126] that if the same couplings are involved in both decays as well as scattering processes, then the former has the dominant contribution to DM relic density over the latter one. The scattering processes have negligibly small contribution to DM relic density [72, 80, 81]. With reference to these past studies, we consider that the dark matter candidate is stable in our model and can produce only from the decay of the heavy vector fermions and Higgs.

The Boltzmann equation for the dark matter can be written as [72, 81, 117],

$$\frac{dn}{dt} + 3Hn = - \sum_i \mathcal{S}(X_{Heavy} \rightarrow SS, f_{SM}S), \quad (4.7)$$

where, $X_{Heavy} = E_1^\pm, E_2^\pm, X_1^0, H$ and f_{SM} is SM leptons. Here, the decay-based source term \mathcal{S} can be written as,

$$\mathcal{S} = \Gamma(X_{Heavy} \rightarrow f_{SM}S, SS) \frac{K_1\left(\frac{m_{X_{Heavy}}}{T}\right)}{K_2\left(\frac{m_{X_{Heavy}}}{T}\right)} n_{Heavy,i}^{eq} \quad (4.8)$$

where, $K_{1,2}$ is the modified Bessel function of the first and second kind. For $x = \frac{m_{X_{Heavy}}}{T}$ and $Y = \frac{n}{T^3}$, the Boltzmann equation from eqn. (4.7) now reads [117],

$$\frac{dY(x)}{dx} = \sum_i \frac{g_{X_{Heavy}}}{2\pi^2} \frac{\Gamma(X_{Heavy} \rightarrow f_{SM}S, SS)}{H(x \approx 1)} x^3 K_1(x), \quad (4.9)$$

where, $g_{X_{Heavy}}$ is the degrees of freedom of the heavy particle. We can integrate the dark matter production over the entire thermal history and look for the final yield $Y(x_0)$ with the help of the appropriate integral [72, 81, 117] as,

$$Y(x_0) = \frac{45 M_{Pl}}{6.64 \pi^4 g^S \sqrt{g^\rho}} \sum_i \frac{g_{X_{Heavy,i}}}{M_{X_{Heavy,i}}^2} \Gamma(X_{Heavy,i} \rightarrow f_{SM} S, SS) \int_{x_{min}}^{x_{max}} x^3 K_1(x) dx, \quad (4.10)$$

with, $g^S, \sqrt{g^\rho}$ are the effective numbers of degrees of freedom in the bath at the freeze-in temperature for the entropy, s , and energy density ρ . Finally the relic density ⁷ ($M_S \equiv M_{DM}$) can be written as [72, 81, 117],

$$\begin{aligned} \Omega h^2 &= \frac{h^2}{3 H_0^2 M_{Pl}^2} \frac{M_S}{28} T_0^3 Y(x_0) \\ &\approx 1.09 \times 10^{27} M_S \sum_i \frac{g_{X_{Heavy,i}} \Gamma(X_{Heavy,i} \rightarrow f_{SM} S, SS)}{M_{X_{Heavy,i}}^2} \end{aligned} \quad (4.11)$$

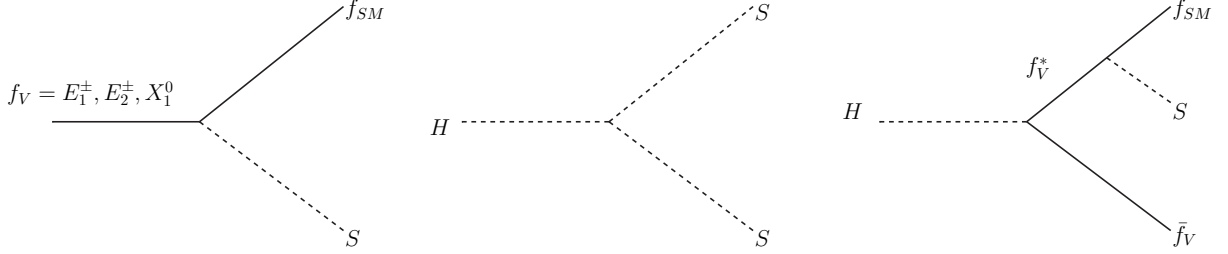


FIG. 6: Dark matter production diagrams from the decay of the heavy particles contribute to the relic density.

We will now follow up the eqn. (4.11) to calculate the relic density. The main production diagrams from the decay of the heavy particles are shown in Fig. 6. The last diagram is kinematically forbidden as we have considered $M_{f_V} \sim 1.5$ TeV. It is to be noted that, the heavy fermion mass of $M_{f_V} \sim 1.5$ TeV can lead to dilepton plus transverse missing energy signature $\gtrsim 3\sigma$ at the LHC for $\sqrt{s} = 14$ TeV with an integrated luminosity 3000 fb^{-1} [105]. The additional four-body decay ($H \rightarrow \bar{f}_V^* f_V^*, f_V^* \rightarrow f_{SM} S \Rightarrow \bar{f}_{SM} f_{SM} SS$) diagram are suppressed by the heavy fermion propagator. The partial decays of the heavy fermions and Higgs into the dark matter particle are given by,

$$\Gamma(f_V \rightarrow f_{SM} S) = \frac{M_{f_V}}{8\pi} |g_{f_V f_{SM} S}|^2 \quad (4.12)$$

⁷ We also crosscheck by using the output of `FeynRules` [119] into `micrOMEGAs` [120] and get the same results.

$$\Gamma(H \rightarrow SS) = \frac{1}{32\pi M_H} |g_{HSS}|^2 \left(1 - \frac{M_S^2}{M_H^2}\right)^{\frac{1}{2}}, \quad (4.13)$$

where, the coupling strengths are (see eqn. 4.7) $g_{HSS} = |\kappa v|$, $g_{SiE_1^\pm} = A_{fi} = |(\cos \beta Y_{fi} + \sin \beta Y'_{fi})|$, $g_{SiE_2^\pm} = B_{fi} = |(\sin \beta Y_{fi} + \cos \beta Y'_{fi})|$ and $g_{S\nu_i X_1^0} = C_{fi} = |Y_{fi}|$, with $i = e, \mu, \tau$.

Now we will discuss the numerical analysis for the FIMP dark matter region of the model parameter spaces. Let us first neglect the contribution from the decay and annihilation from the scalar sector, i.e., $\kappa = 0$, hence $\Gamma(H \rightarrow SS) = 0$ and $\sigma(\text{SM particles} \rightarrow SS) = 0$. It is to be noted that the mass of the dark matter can be set by the independent parameter m_S (see eqn. (2.6)). We find that the t -channel annihilation processes $\sigma(f_V f_V \rightarrow SS)$ through f_{SM} propagator and $\sigma(f_{\text{SM}} f_{\text{SM}} \rightarrow SS)$ through f_V propagator are also suppresses as compared to the decay $\Gamma(f_V \rightarrow f_{\text{SM}} S)$ contributions. The variation of the new vector-like Yukawa coupling Y_{fi}

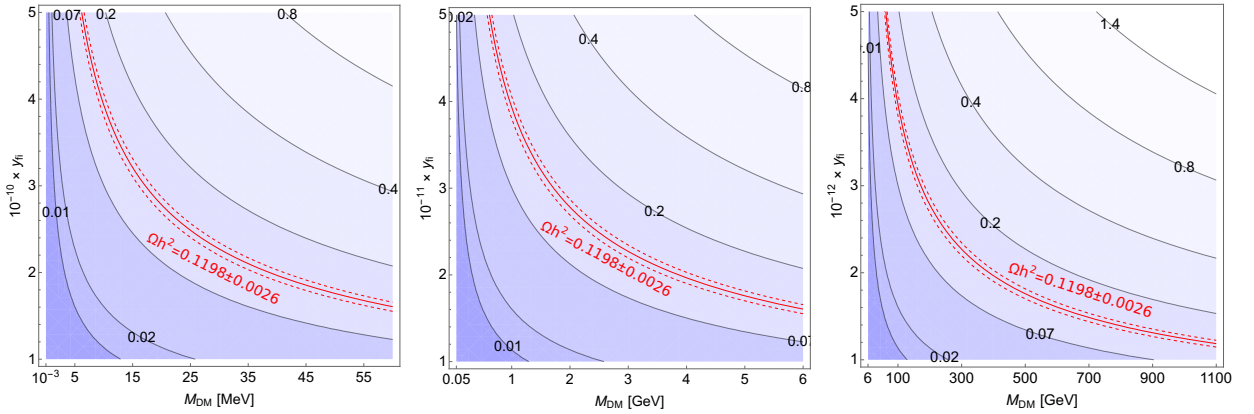


FIG. 7: The contour lines stand for the relic density in the new Yukawa coupling vs. dark matter mass plane. The red-lines indicate the relic density within the 3σ range. These region with $Y_{fi} \ll 1$ are also allowed by the recent LFV [114] $BR(\mu \rightarrow e\gamma) < 4.2 \times 10^{-13}$ at 90% CL, electron as well as muon anomalous magnetic moment $g - 2$ data at Fermilab [83]. The masses $M_{E_1^\pm} = 1500$ GeV and $M_{E_2^\pm} = 3000$ GeV and $\cos \beta = 0.995$, hence $M_{X_1^0} = 1514.9625$ GeV.

($i = e, \mu, \tau$) with the mass of the dark matter are shown in Fig. 7. In the meanwhile, we have neglected the effect from the interaction term $-Y'_{fi} \bar{l}_{i,R} E_S S$ by considering $Y'_{fi} = 0$ in these plots. The dominant contributions ($> 95\%$) to the relic density mainly come from the decay of the fermions E_1^\pm and X_1^0 . In both plots, the solid red line represents $\Omega h^2 = 0.1198$, and the red dashed lines correspond to the 3σ variation in Ωh^2 . The lighter region corresponds to higher values of Ωh^2 , which over close the universe and these regions strictly forbidden. The left plot is kept for the dark matter mass region $M_S \equiv M_{DM} = 6$ MeV to 60 MeV, whereas the right plot corresponds to the dark matter mass region 60 MeV to 6 GeV. One can also get the exact relic density for the dark matter mass $\mathcal{O}(1)$ keV region, but it will create a problem for the structure formation. We

calculate the free streaming length by following the formula given in equation (14) of the Ref. [127],

$$\lambda_{FS} = \int_{a_{FS}}^1 \frac{da}{H_0 F(a)} \frac{\langle p_{DM} \rangle a_{FS}}{\sqrt{(\langle p_{DM} \rangle a_{FS})^2 + (m_{DM} a)^2}}, \quad (4.14)$$

where, $F(a) = \sqrt{\Omega_{rad,0} + a\Omega_{m,0} + a^4\Omega_{\Lambda,0}}$. We get $\langle p_{DM} \rangle \approx \frac{M_H}{2}$ and a_{FS} is calculated by equating the decay rate of the Higgs into two DM ($\Gamma(H \rightarrow SS)$) to the Hubble expansion rate $H \approx \frac{T^2}{M_{Planck}}$ during radiation dominated era and H_0 is the present Hubble expansion rate. The latest values of the cosmological parameters can be found in Ref. [128]. We find the free streaming length larger than 10 Mpc; hence, we avoid showing these regions in this analysis. We also calculate the free streaming length [127, 129] of the dark matter particles, and it is coming out to be less than $\mathcal{O}(100)$ kpc in the parameter space we have shown in both plots of Fig. 7. Therefore, the dark matter still behave like a cold one [129]. For the heavier dark matter mass region, we need smaller Yukawa coupling as it compensate by the dark matter mass in the decay width. For example, we get the relic density in the right ballpark for $Y_{fi} = 1.244 \times 10^{-9}$ with $M_{DM} = 1$ MeV and $Y_{fi} = 1.759 \times 10^{-10}$ with $M_{DM} = 50$ MeV and we also get the relic density in the right ballpark for $Y_{fi} = 3.935 \times 10^{-11}$ with $M_{DM} = 1$ GeV and $Y_{fi} = 1.759 \times 10^{-11}$ with $M_{DM} = 5$ GeV. Hence, we get the relic density for $Y_{fi} \sim \mathcal{O}(10^{-10})$ through the Freeze-in scenario, and the contributions are tiny $\mathcal{O}(10^{-32})$ to the recent LFV $BR(\mu \rightarrow e\gamma)$ [114], electron as well as muon anomalous magnetic moment [83] $g - 2$ data.

We also change the mixing angle from $\cos \beta = 0.995$ to $\cos \beta = 0.60$, keep fixed value of the masses $M_{E_1^\pm} = 1500$ GeV and $M_{E_2^\pm} = 3000$ GeV. We find a tiny change in the relic density; however, the plots in Fig. 7 remain almost the same. Remarkably, the relic density gets hugely modified for the WIMP dark matter scenario in the Freeze-out mechanism, and they are shown in Fig. 5. The effect of the mixing angle is almost negligible in this Freeze-in mechanism where the dark matter gets produce from the decay of the heavy particles. For the fixed value of $\cos \beta = 0.995$ and $M_{E_1^\pm} = 1500$ GeV, one can also varied the mass $M_{E_2^\pm}$, we find a very small effect in the relic density as the decay rate of E_2^\pm is far smaller than the decay rate of E_1^\pm .

We now consider the contributions from the Higgs decay in the relic density. In this case, we still assume $Y'_{fi} = 0$, to diminish the contributions from decay of E_2^\pm . The larger κ increases the Higgs decays' contributions, whereas large values of Y_{fi} increases the contributions from the vector-like fermions E_1^\pm and X_1^0 . We show such variations for two different dark matter masses $M_{DM} = 1$ MeV and 1 GeV respectively in Fig. 8. The solid red line in both plots corresponds $\Omega h^2 = 0.1198$, and the red dashed lines represent the 3σ variation in Ωh^2 . The lighter region will over close the Universe. Therefore, very small $\kappa = \mathcal{O}(10^{-10})$ and $Y_{fi} = \mathcal{O}(10^{-10})$ are needed to get the exact relic density in the right ballpark. The additional fine-tune issues in these low dark matter mass regions are: (a) How could one get such a small dark matter mass? (b) How could

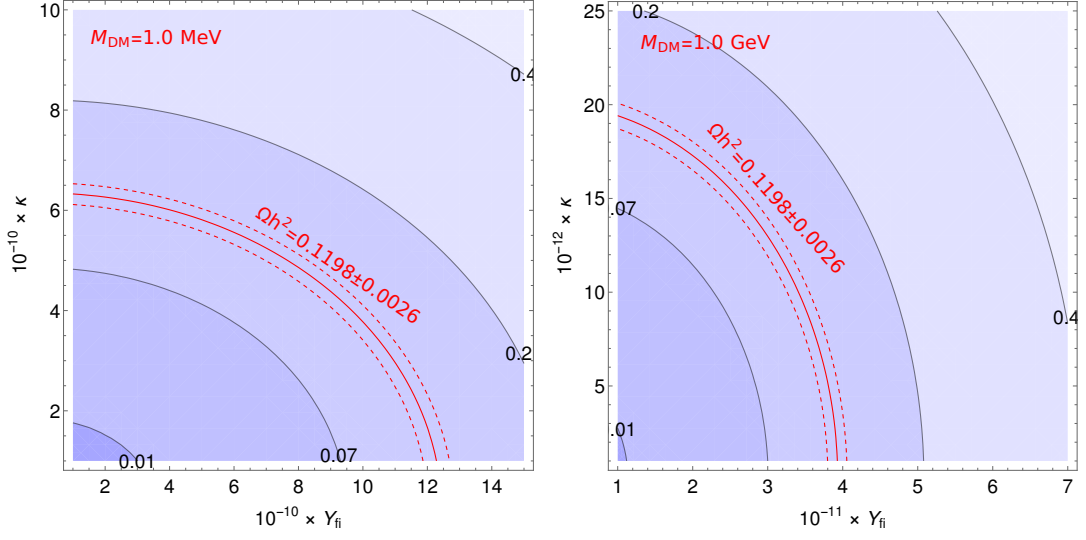


FIG. 8: The contour lines stand for the relic density in the new Yukawa coupling vs. dark matter mass plane. The red-lines indicate the relic density within the 3σ range. These region are also allowed by the recent LFV, electron as well as muon anomalous magnetic moment $g - 2$ data. The masses $M_{E_1^\pm} = 1500$ GeV and $M_{E_2^\pm} = 3000$ GeV and $\cos \beta = 0.995$, hence $M_{X_1^0} = 1514.9625$ GeV.

one get such small couplings? One of the answers might be the Freeze-in mechanism for FIMP dark matter, and we need small coupling and mass to get the exact relic density. In the following collider section, we will discuss, whether it is possible to put additional constraints on DM mass from the indirect dark matter detection and/or from the collider experiments, if we have a tiny dark matter mass.

Now, we check the effect for the interaction term $Y'_{fi} \bar{l}_{i,R} E_S S$ with $Y'_{fi} \neq 0$. It will increase the contribution from the second charged fermion E_2^\pm . If we assume the $Y_{fi} = 0$ and $\kappa = 0$, then in the relic density, the dominant contribution come from the decay of this charged fermion E_2^\pm . In Fig. 9, we show the contour regions for the relic density in Y'_{fi} vs. dark matter mass (both MeV and GeV region) plane. The red lines within the 3σ range. The contribution from the other charged fermion E_1^\pm is less than one percent for this choice of $\cos \beta = 0.995$.

In the presence of Y_{fi} and κ , one can have additional contributions to the relic density from the decay of charged fermion E_1^\pm and Higgs scalar. In these two contour plot in Fig. 10, we keep x-axis reserve for Y'_{fi} and y-axis for Y_{fi} and κ respectively. We neglect the contribution from the Higgs decay in the left plot of Fig. 10, i.e., $\kappa = 0$ whereas the $Y_{fi} = 0$ in right plot. We consider fixed dark matter mass at 1 MeV and we keep $\cos \beta = 0.995$, $M_{E_1^\pm} = 1500$ GeV and $M_{E_2^\pm} = 3000$ GeV.

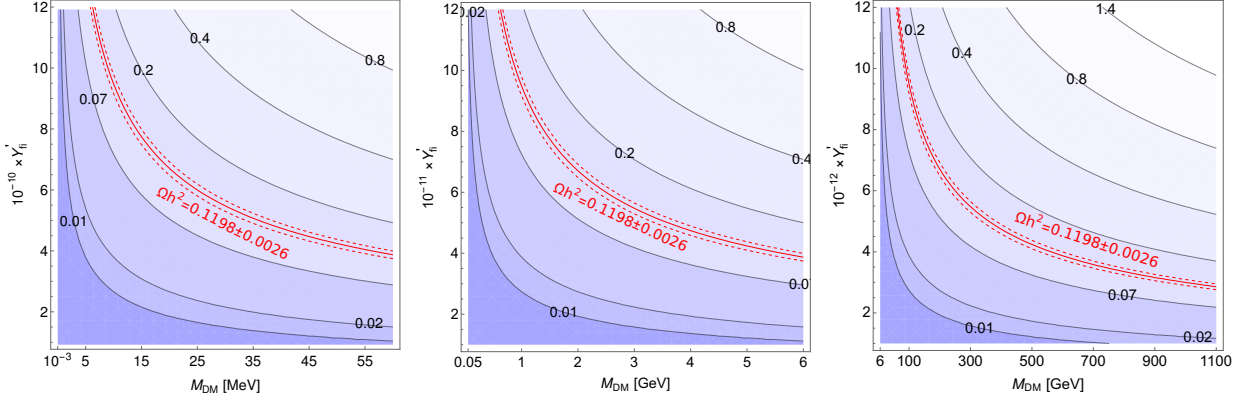


FIG. 9: The contour lines stand for the relic density in the new Yukawa coupling vs. dark matter mass plane. The red-lines indicate the relic density within the 3σ range.

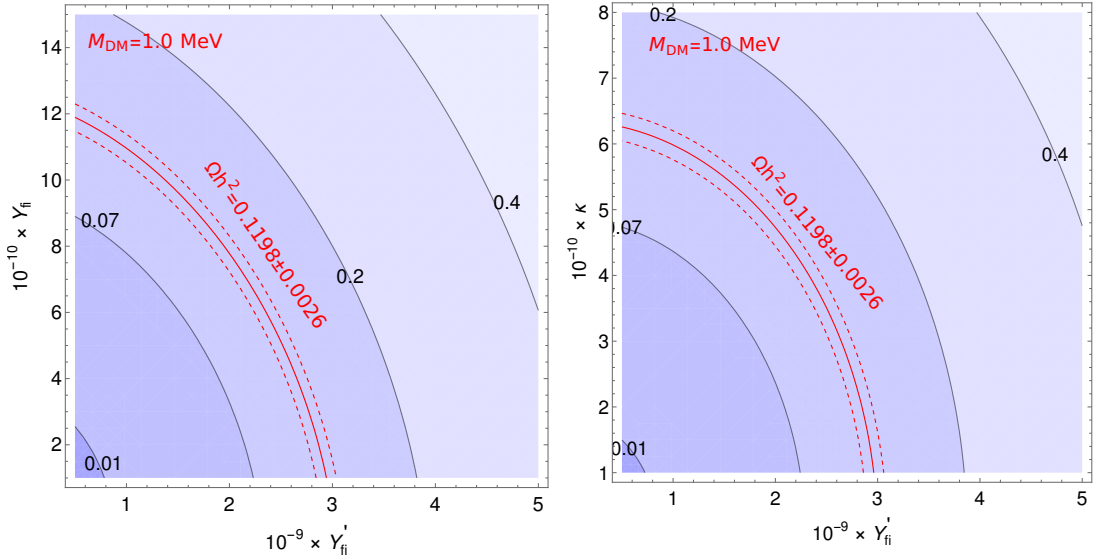


FIG. 10: The contour lines stand for the relic density in the new Yukawa coupling (Y'_{fi}) vs. the old Yukawa coupling (Y_{fi}) and κ respectively. The red-lines indicate the relic density within the 3σ range.

V. INDIRECT DETECTION LIMITS

The normal gamma-ray limits from the Fermi-LAT do not apply for the mass $< \mathcal{O}(100)$ MeV, although the data from several other satellites such as HEAO-1 [130], INTEGRAL [131], COMPTEL [132], EGRET [133] are extremely sensitive to photons with energies well below a $\mathcal{O}(100)$ MeV. For a DM annihilation spectrum dN_γ/dE , and a galactic DM density profile $\rho(r)$, the galactic

contribution to the differential photon flux per unit energy is given by [134],

$$\frac{d\Phi_{\gamma,G}}{dEd\Omega} = \frac{r_{\odot} \rho_{\odot} \Gamma_A}{4\pi 2^{\alpha-1} M_{DM}} J_{D,A} \frac{dN_{\gamma}}{dE}, \quad (5.1)$$

where, $\Gamma_A = \frac{\rho_{\odot}}{M_{DM}} \langle \sigma v_{DM} \rangle$, $r_{\odot} \sim 8.5$ kpc is the Sun's distance from the Galactic center and $\rho_{\odot} = 0.3 \text{ GeV cm}^{-3}$ is the local DM density. $\alpha = 1(2)$ for DM decays (annihilations) and $J_A = \int_{l.o.s} \frac{ds}{r_{\odot}} \left(\frac{\rho(s)}{\rho_{\odot}} \right)^{\alpha}$ is a dimensionless quantity that describes the density of decays or annihilations along the line-of-sight (l.o.s.), and $\rho(s) = \rho(r, l, b)$ can be found in [135]. The extra-galactic photon spectrum arising from dark matter decays; thus, the contribution is zero here. The $E^2 \frac{d\Phi_{\gamma,Tot}}{dEd\Omega}$ vs. E limits are shown in Fig. 1 of the Ref. [134]. We find the average dark matter annihilation cross-section $\langle \sigma v_{DM} \rangle \approx 10^{-64} \text{ cm}^3/\text{s}$ in the exact relic density region. We have found that to explain above experimental data, we need a very large $\kappa \sim Y_{fl} \sim 25$ which violates perturbativity. Hence, the regions considered in this analysis are allowed from these experimental limits.

VI. DIRECT DETECTION AT COLLIDER AS CHARGED TRACK

As we have mentioned that we need a tiny Higgs portal coupling $\kappa \sim 10^{-10}$ to get the exact relic density; hence, the direct detection limit (e.g., XENON-IT limit [73]) is not applicable for the FIMP dark matter. The detailed collider bounds have been discussed in our previous paper [105] for the same model in the context of WIMP scenario. The authors of the Ref. [136] have discussed the method to prob the FIMP dark matter in the recent LHC collider with high integrated luminosity using the MATHUSLA surface detector. A charged track can be obtained in this model due to the vector fermions' decay into SM fermion and dark matter candidate at the collider. In this model, the length travelled by the charged fermion $E_{1,2}^{\pm}$ before its decay.

$$c\tau_{E_{1,2}^{\pm}} = \frac{4.9627 \times 10^{-13}}{g_{fV}^2} \left(\frac{1 \text{ [GeV]}}{M_{E_{1,2}^{\pm}}} \right) \text{ cm}. \quad (6.1)$$

Can we get enough events from this charged track? It mainly depends on the production cross-section $\sigma_{\sqrt{s}}^{\text{LHC}}$ of the mother particle (vector fermion or Higgs) and luminosity \mathcal{L} at the detector. The number of events at the LHC is calculated in Ref. [136], and it is given by

$$N_{events} = \sigma_{\sqrt{s}}^{\text{LHC}} \mathcal{L} \int P_{\text{Decay}}^{\text{MATH}}, \quad \text{with} \quad P_{\text{Decay}}^{\text{MATH}} = 0.05 \left(e^{-\frac{L_a}{\beta c \tau_{fMF}}} - e^{-\frac{L_b}{\beta c \tau_{fMF}}} \right), \quad (6.2)$$

The author of Ref. [136], find the number of events $N_{events} \geq 3$ for $\sqrt{s} = 13$ TeV with an integrated luminosity $\mathcal{L} = 3000 \text{ fb}^{-1}$ using their model parameter spaces. They showed that the MATHUSLA100/200 detector could detect these mother particle up to 1 TeV. The dominant

production of the vector fermions come through the Drell-Yan processes.

In this model, we find the production cross-section of the vector like charged fermions with mass $M_{E_1^\pm} = 1500$ GeV is 6.53×10^{-3} fb [105]. Hence we need large luminosity and/or energy to get a significant event at the present MATHUSLA100/200 surface detector. We find $N_{events} > 3$ at 14 TeV LHC with an integrated luminosity $\mathcal{L} = 10^6$ fb $^{-1}$. The 14 TeV HL-LHC will collect data around 3000 fb $^{-1}$, so this search will not be effective. We need wait for the 100 TeV with high luminosity collider.

VII. CONCLUSION

In this work, we study the possibility of dark matter in an extended singlet scalar model. The structure of the model shown here uses a minimum number of particle content. This model contains two additional vector-like charged fermion and a neutral fermion along with a real singlet scalar field. In the previous study [105], we have added one extra vector-like fermion doublet in the model to complete the neutrino framework. We also see that the additional heavy vector-like fermions from this doublet do not alter the dark matter phenomenology as the mixing was taken to be very small. However, the neutrino sector is skipped in this work and rather focus on the WIMP and FIMP dark matter analysis.

We revisited the dark matter analysis through a Freeze-out mechanism considering the collider bound as discussed in Ref. [105]. Here, we show a broad region of the WIMP dark matter parameter spaces which satisfy the relic density at the right ballpark. We choose different dark matter parameter spaces to get the new allowed region from the relic density through the Freeze-out mechanism. In the presence of vector-like fermions, one can get the correct relic density via co-annihilation, or one may have the interaction term such that the dark matter can annihilate into SM particles through additional cross-channel, t - and u -channels. The destructive and/or constructive interference among these channels helps to modify the effective average dark matter annihilation cross-section and provide the exact relic density in this model.

This study also focuses on the low dark matter parameter spaces where the dark matter density can explain through the Freeze-in mechanism. As we know, one cannot get the same viable dark matter parameter space in the low dark matter region as it will either violate the relic density, direct detection constraints or the perturbative limit. Interestingly, in this study, we showed that a single model could explain the low and high dark matter mass region allowed from all the other phenomenological constraints. If, in the future, we able to get any signature at a very low or high dark matter mass region (keV-TeV mass region), our present (including the previous) study could help in estimating a better parameter space.

A few comments on the recent muon anomalous magnetic moment experimental results are made in this model. We see that both the charged particles and the dark matter candidate

played a crucial role in providing additional contributions. It was found that one can explain the experimental data throughout the parameter spaces. However, the lepton violating decay channels, perturbative and unitary limits put stringent constraints on the parameter spaces. The dark matter mass region allowed by relic density through Freeze-in and Freeze-out mechanisms is also allowed by the recent muon $g - 2$ data at Fermilab. However, the converse is not valid in our model, as the region allowed by muon $g - 2$ data violates the relic density bound. We also perform the collider analysis to search the new particles in the FIMP like scenario in the context of the same 14 TeV LHC experiments with the MATHUSLA100/200 detector. A charged track can be obtained due to the decay of the heavy charged fermion $E_{1,2}^\pm$ into SM fermion and dark matter. One can get events larger than $N = 3$, when the LHC operated with integrated luminosity $\mathcal{L} = 10^6 \text{ fb}^{-1}$.

VIII. ACKNOWLEDGEMENTS

The research work of P.D. and M.K.D. is supported by the Department of Science and Technology, Government of India under the project grant EMR/2017/001436. NK would like to thank to Prof. Dilip Kumar Ghosh for his support at IACS. This project has also received funding/support from the European Union’s Horizon 2020 research and innovation programme under the Marie Skłodowska -Curie grant agreement No 860881-HIDDeN”.

-
- [1] E. W. Kolb and M. S. Turner, *The Early Universe*, vol. 69. 1990.
 - [2] **CMS** Collaboration, A. M. Sirunyan *et al.*, “Observation of the Higgs boson decay to a pair of τ leptons with the CMS detector,” *Phys. Lett.* **B779** (2018) 283–316, [arXiv:1708.00373 \[hep-ex\]](#).
 - [3] **CMS** Collaboration, A. M. Sirunyan *et al.*, “Combined measurements of Higgs boson couplings in proton–proton collisions at $\sqrt{s} = 13 \text{ TeV}$,” *Eur. Phys. J.* **C79** no. 5, (2019) 421, [arXiv:1809.10733 \[hep-ex\]](#).
 - [4] L. J. Hall, K. Jedamzik, J. March-Russell, and S. M. West, “Freeze-In Production of FIMP Dark Matter,” *JHEP* **03** (2010) 080, [arXiv:0911.1120 \[hep-ph\]](#).
 - [5] **XENON** Collaboration, E. Aprile *et al.*, “Dark Matter Search Results from a One Ton-Year Exposure of XENON1T,” *Phys. Rev. Lett.* **121** no. 11, (2018) 111302, [arXiv:1805.12562 \[astro-ph.CO\]](#).
 - [6] **Planck** Collaboration, N. Aghanim *et al.*, “Planck 2018 results. VI. Cosmological parameters,” [arXiv:1807.06209 \[astro-ph.CO\]](#).
 - [7] C. P. Burgess, M. Pospelov, and T. ter Veldhuis, “The Minimal model of nonbaryonic dark matter: A Singlet scalar,” *Nucl. Phys.* **B619** (2001) 709–728, [arXiv:hep-ph/0011335 \[hep-ph\]](#).

- [8] N. G. Deshpande and E. Ma, “Pattern of Symmetry Breaking with Two Higgs Doublets,” *Phys. Rev. D* **18** (1978) 2574.
- [9] N. Khan, “Exploring the hyperchargeless Higgs triplet model up to the Planck scale,” *Eur. Phys. J. C* **78** no. 4, (2018) 341, [arXiv:1610.03178 \[hep-ph\]](#).
- [10] A. Chaudhuri, N. Khan, B. Mukhopadhyaya, and S. Rakshit, “Dark matter candidate in an extended type III seesaw scenario,” *Phys. Rev. D* **91** (2015) 055024, [arXiv:1501.05885 \[hep-ph\]](#).
- [11] K. R. Dienes and B. Thomas, “Dynamical Dark Matter: I. Theoretical Overview,” *Phys. Rev. D* **85** (2012) 083523, [arXiv:1106.4546 \[hep-ph\]](#).
- [12] D. Borah, B. Karmakar, and D. Nanda, “Common Origin of Dirac Neutrino Mass and Freeze-in Massive Particle Dark Matter,” *JCAP* **07** (2018) 039, [arXiv:1805.11115 \[hep-ph\]](#).
- [13] A. Biswas and A. Gupta, “Freeze-in Production of Sterile Neutrino Dark Matter in $U(1)_{B-L}$ Model,” *JCAP* **09** (2016) 044, [arXiv:1607.01469 \[hep-ph\]](#). [Addendum: *JCAP* **05**, A01 (2017)].
- [14] F. Elahi, C. Kolda, and J. Unwin, “UltraViolet Freeze-in,” *JHEP* **03** (2015) 048, [arXiv:1410.6157 \[hep-ph\]](#).
- [15] **Muon g-2** Collaboration, B. Abi *et al.*, “Measurement of the Positive Muon Anomalous Magnetic Moment to 0.46 ppm,” *Phys. Rev. Lett.* **126** (2021) 141801, [arXiv:2104.03281 \[hep-ex\]](#).
- [16] **Muon g-2** Collaboration, G. W. Bennett *et al.*, “Final Report of the Muon E821 Anomalous Magnetic Moment Measurement at BNL,” *Phys. Rev. D* **73** (2006) 072003, [arXiv:hep-ex/0602035](#).
- [17] R. H. Parker, C. Yu, W. Zhong, B. Estey, and H. Müller, “Measurement of the fine-structure constant as a test of the Standard Model,” *Science* **360** (2018) 191, [arXiv:1812.04130 \[physics.atom-ph\]](#).
- [18] J. Aebischer, W. Dekens, E. E. Jenkins, A. V. Manohar, D. Sengupta, and P. Stoffer, “Effective field theory interpretation of lepton magnetic and electric dipole moments,” [arXiv:2102.08954 \[hep-ph\]](#).
- [19] T. Abe, R. Sato, and K. Yagyu, “Muon specific two-Higgs-doublet model,” *JHEP* **07** (2017) 012, [arXiv:1705.01469 \[hep-ph\]](#).
- [20] E. J. Chun and J. Kim, “Leptonic Precision Test of Leptophilic Two-Higgs-Doublet Model,” *JHEP* **07** (2016) 110, [arXiv:1605.06298 \[hep-ph\]](#).
- [21] S. Baek, N. Deshpande, X. He, and P. Ko, “Muon anomalous g-2 and gauged $L(\mu) - L(\tau)$ models,” *Phys. Rev. D* **64** (2001) 055006, [arXiv:hep-ph/0104141](#).
- [22] M. Endo, K. Hamaguchi, and G. Mishima, “Constraints on Hidden Photon Models from Electron g-2 and Hydrogen Spectroscopy,” *Phys. Rev. D* **86** (2012) 095029, [arXiv:1209.2558 \[hep-ph\]](#).
- [23] Y. Abe, T. Toma, and K. Tsumura, “A μ - τ -philic scalar doublet under Z_n flavor symmetry,” *JHEP* **06** (2019) 142, [arXiv:1904.10908 \[hep-ph\]](#).

- [24] S. Jana, P. K. Vishnu, W. Rodejohann, and S. Saad, “Dark matter assisted lepton anomalous magnetic moments and neutrino masses,” *Phys. Rev. D* **102** no. 7, (2020) 075003, [arXiv:2008.02377 \[hep-ph\]](#).
- [25] D. Sabatta, A. S. Cornell, A. Goyal, M. Kumar, B. Mellado, and X. Ruan, “Connecting muon anomalous magnetic moment and multi-lepton anomalies at LHC,” *Chin. Phys. C* **44** no. 6, (2020) 063103, [arXiv:1909.03969 \[hep-ph\]](#).
- [26] S. von Buddenbrock, N. Chakrabarty, A. S. Cornell, D. Kar, M. Kumar, T. Mandal, B. Mellado, B. Mukhopadhyaya, R. G. Reed, and X. Ruan, “Phenomenological signatures of additional scalar bosons at the LHC,” *Eur. Phys. J. C* **76** no. 10, (2016) 580, [arXiv:1606.01674 \[hep-ph\]](#).
- [27] L. Calibbi, R. Ziegler, and J. Zupan, “Minimal models for dark matter and the muon $g-2$ anomaly,” *JHEP* **07** (2018) 046, [arXiv:1804.00009 \[hep-ph\]](#).
- [28] N. Chen, B. Wang, and C.-Y. Yao, “The collider tests of a leptophilic scalar for the anomalous magnetic moments,” [arXiv:2102.05619 \[hep-ph\]](#).
- [29] W. Yin, “Radiative lepton mass and muon $g-2$ with suppressed lepton flavor and CP violations,” [arXiv:2103.14234 \[hep-ph\]](#).
- [30] E. J. Chun and T. Mondal, “Searching for a Light Higgs Boson via the Yukawa Process at Lepton Colliders,” *Phys. Lett. B* **802** (2020) 135190, [arXiv:1909.09515 \[hep-ph\]](#).
- [31] K. S. Babu, “TASI Lectures on Flavor Physics,” in *Proceedings of Theoretical Advanced Study Institute in Elementary Particle Physics on The dawn of the LHC era (TASI 2008): Boulder, USA, June 2-27, 2008*, pp. 49–123. 2010. [arXiv:0910.2948 \[hep-ph\]](#).
- [32] E. Ma and D. Suematsu, “Fermion Triplet Dark Matter and Radiative Neutrino Mass,” *Mod. Phys. Lett. A* **24** (2009) 583–589, [arXiv:0809.0942 \[hep-ph\]](#).
- [33] T. Araki, C. Q. Geng, and K. I. Nagao, “Dark Matter in Inert Triplet Models,” *Phys. Rev.* **D83** (2011) 075014, [arXiv:1102.4906 \[hep-ph\]](#).
- [34] A. Das, T. Nomura, H. Okada, and S. Roy, “Generation of a radiative neutrino mass in the linear seesaw framework, charged lepton flavor violation, and dark matter,” *Phys. Rev. D* **96** no. 7, (2017) 075001, [arXiv:1704.02078 \[hep-ph\]](#).
- [35] E. Ma, “Verifiable radiative seesaw mechanism of neutrino mass and dark matter,” *Phys. Rev.* **D73** (2006) 077301, [arXiv:hep-ph/0601225 \[hep-ph\]](#).
- [36] S. Bhattacharya, N. Sahoo, and N. Sahu, “Singlet-Doublet Fermionic Dark Matter, Neutrino Mass and Collider Signatures,” *Phys. Rev. D* **96** no. 3, (2017) 035010, [arXiv:1704.03417 \[hep-ph\]](#).
- [37] P. Das, M. K. Das, and N. Khan, “A new feasible dark matter region in the singlet scalar scotogenic model,” *Nucl. Phys. B* **964** (2021) 115307, [arXiv:2001.04070 \[hep-ph\]](#).
- [38] T. Cohen, J. Kearney, A. Pierce, and D. Tucker-Smith, “Singlet-Doublet Dark Matter,” *Phys. Rev.* **D85** (2012) 075003, [arXiv:1109.2604 \[hep-ph\]](#).

- [39] K. Griest and M. Kamionkowski, “Unitarity Limits on the Mass and Radius of Dark Matter Particles,” *Phys. Rev. Lett.* **64** (1990) 615.
- [40] K. Kowalska and E. M. Sessolo, “Expectations for the muon $g-2$ in simplified models with dark matter,” *JHEP* **09** (2017) 112, [arXiv:1707.00753 \[hep-ph\]](#).
- [41] K. Kowalska and E. M. Sessolo, “Minimal models for $g-2$ and dark matter confront asymptotic safety,” [arXiv:2012.15200 \[hep-ph\]](#).
- [42] J. Kawamura, S. Okawa, and Y. Omura, “Current status and muon $g-2$ explanation of lepton portal dark matter,” *JHEP* **08** (2020) 042, [arXiv:2002.12534 \[hep-ph\]](#).
- [43] M. J. Baker, P. Cox, and R. R. Volkas, “Radiative muon mass models and $(g-2)_\mu$,” *JHEP* **05** (2021) 174, [arXiv:2103.13401 \[hep-ph\]](#).
- [44] P. B. Pal, *An introductory course of particle physics*. Taylor & Francis, 2014.
- [45] F. Pisano and A. T. Tran, “Anomaly cancellation in a class of chiral flavor gauge models,” in *14th Brazilian Meeting on Particles and Fields*. 7, 1993.
- [46] **MEG II** Collaboration, A. M. Baldini *et al.*, “The design of the MEG II experiment,” *Eur. Phys. J. C* **78** no. 5, (2018) 380, [arXiv:1801.04688 \[physics.ins-det\]](#).
- [47] W. Chao, “The Muon Magnetic Moment in the TeV Scale Seesaw Models,” [arXiv:0806.0889 \[hep-ph\]](#).
- [48] C.-H. Chen and T. Nomura, “Influence of an inert charged Higgs boson on the muon $g-2$ and radiative neutrino masses in a scotogenic model,” *Phys. Rev. D* **100** no. 1, (2019) 015024, [arXiv:1903.03380 \[hep-ph\]](#).
- [49] M. Bauer and T. Plehn, *Yet Another Introduction to Dark Matter: The Particle Physics Approach*, vol. 959 of *Lecture Notes in Physics*. Springer, 2019. [arXiv:1705.01987 \[hep-ph\]](#).
- [50] P. Gondolo and G. Gelmini, “Cosmic abundances of stable particles: Improved analysis,” *Nucl. Phys. B* **360** (1991) 145–179.
- [51] A. Alloul, N. D. Christensen, C. Degrande, C. Duhr, and B. Fuks, “FeynRules 2.0 - A complete toolbox for tree-level phenomenology,” *Comput. Phys. Commun.* **185** (2014) 2250–2300, [arXiv:1310.1921 \[hep-ph\]](#).
- [52] G. Bélanger, F. Boudjema, A. Goudelis, A. Pukhov, and B. Zaldivar, “micrOMEGAs5.0 : Freeze-in,” *Comput. Phys. Commun.* **231** (2018) 173–186, [arXiv:1801.03509 \[hep-ph\]](#).
- [53] F. Staub, “Exploring new models in all detail with SARAH,” *Adv. High Energy Phys.* **2015** (2015) 840780, [arXiv:1503.04200 \[hep-ph\]](#).
- [54] W. Porod and F. Staub, “SPHeno 3.1: Extensions including flavour, CP-phases and models beyond the MSSM,” *Comput. Phys. Commun.* **183** (2012) 2458–2469, [arXiv:1104.1573 \[hep-ph\]](#).
- [55] K. Griest and D. Seckel, “Three exceptions in the calculation of relic abundances,” *Phys. Rev. D* **43** (1991) 3191–3203.

- [56] N. Arkani-Hamed, D. P. Finkbeiner, T. R. Slatyer, and N. Weiner, “A Theory of Dark Matter,” *Phys. Rev.* **D79** (2009) 015014, [arXiv:0810.0713 \[hep-ph\]](#).
- [57] C. E. Yaguna, “The Singlet Scalar as FIMP Dark Matter,” *JHEP* **08** (2011) 060, [arXiv:1105.1654 \[hep-ph\]](#).
- [58] N. Bernal, M. Heikinheimo, T. Tenkanen, K. Tuominen, and V. Vaskonen, “The Dawn of FIMP Dark Matter: A Review of Models and Constraints,” *Int. J. Mod. Phys.* **A32** no. 27, (2017) 1730023, [arXiv:1706.07442 \[hep-ph\]](#).
- [59] G. Choi, T. T. Yanagida, and N. Yokozaki, “Feebly interacting $U(1)_{B-L}$ gauge boson warm dark matter and XENON1T anomaly,” *Phys. Lett. B* **810** (2020) 135836, [arXiv:2007.04278 \[hep-ph\]](#).
- [60] **Planck** Collaboration, N. Aghanim *et al.*, “Planck 2018 results. VI. Cosmological parameters,” *Astron. Astrophys.* **641** (2020) A6, [arXiv:1807.06209 \[astro-ph.CO\]](#). [Erratum: *Astron. Astrophys.* 652, C4 (2021)].
- [61] P. S. Bhupal Dev, A. Mazumdar, and S. Qutub, “Constraining Non-thermal and Thermal properties of Dark Matter,” *Front. in Phys.* **2** (2014) 26, [arXiv:1311.5297 \[hep-ph\]](#).
- [62] D. Gruber, J. Matteson, L. Peterson, and G. Jung, “The spectrum of diffuse cosmic hard x-rays measured with heao-1,” *Astrophys. J.* **520** (1999) 124, [arXiv:astro-ph/9903492](#).
- [63] L. Bouchet, E. Jourdain, J. Roques, A. Strong, R. Diehl, F. Lebrun, and R. Terrier, “INTEGRAL SPI All-Sky View in Soft Gamma Rays: Study of Point Source and Galactic Diffuse Emissions,” *Astrophys. J.* **679** (2008) 1315, [arXiv:0801.2086 \[astro-ph\]](#).
- [64] K. S. C., *Ph. D. Thesis*. PhD thesis, University of New Hampshire, USA, 1998.
- [65] A. W. Strong, I. V. Moskalenko, and O. Reimer, “Diffuse galactic continuum gamma rays. A Model compatible with EGRET data and cosmic-ray measurements,” *Astrophys. J.* **613** (2004) 962–976, [arXiv:astro-ph/0406254](#).
- [66] R. Essig, E. Kuflik, S. D. McDermott, T. Volansky, and K. M. Zurek, “Constraining Light Dark Matter with Diffuse X-Ray and Gamma-Ray Observations,” *JHEP* **11** (2013) 193, [arXiv:1309.4091 \[hep-ph\]](#).
- [67] J. F. Navarro, C. S. Frenk, and S. D. White, “A Universal density profile from hierarchical clustering,” *Astrophys. J.* **490** (1997) 493–508, [arXiv:astro-ph/9611107](#).
- [68] J. M. No, P. Tunney, and B. Zaldivar, “Probing Dark Matter freeze-in with long-lived particle signatures: MATHUSLA, HL-LHC and FCC-hh,” *JHEP* **03** (2020) 022, [arXiv:1908.11387 \[hep-ph\]](#).
- [69] E. W. Kolb and M. S. Turner, *The Early Universe*, vol. 69. 1990.
- [70] **CMS** Collaboration, A. M. Sirunyan *et al.*, “Observation of the Higgs boson decay to a pair of τ leptons with the CMS detector,” *Phys. Lett.* **B779** (2018) 283–316, [arXiv:1708.00373 \[hep-ex\]](#).

- [71] **CMS** Collaboration, A. M. Sirunyan *et al.*, “Combined measurements of Higgs boson couplings in proton–proton collisions at $\sqrt{s} = 13$ TeV,” *Eur. Phys. J.* **C79** no. 5, (2019) 421, [arXiv:1809.10733 \[hep-ex\]](#).
- [72] L. J. Hall, K. Jedamzik, J. March-Russell, and S. M. West, “Freeze-In Production of FIMP Dark Matter,” *JHEP* **03** (2010) 080, [arXiv:0911.1120 \[hep-ph\]](#).
- [73] **XENON** Collaboration, E. Aprile *et al.*, “Dark Matter Search Results from a One Ton-Year Exposure of XENON1T,” *Phys. Rev. Lett.* **121** no. 11, (2018) 111302, [arXiv:1805.12562 \[astro-ph.CO\]](#).
- [74] **Planck** Collaboration, N. Aghanim *et al.*, “Planck 2018 results. VI. Cosmological parameters,” [arXiv:1807.06209 \[astro-ph.CO\]](#).
- [75] C. P. Burgess, M. Pospelov, and T. ter Veldhuis, “The Minimal model of nonbaryonic dark matter: A Singlet scalar,” *Nucl. Phys.* **B619** (2001) 709–728, [arXiv:hep-ph/0011335 \[hep-ph\]](#).
- [76] N. G. Deshpande and E. Ma, “Pattern of Symmetry Breaking with Two Higgs Doublets,” *Phys. Rev.* **D18** (1978) 2574.
- [77] N. Khan, “Exploring the hyperchargeless Higgs triplet model up to the Planck scale,” *Eur. Phys. J.* **C78** no. 4, (2018) 341, [arXiv:1610.03178 \[hep-ph\]](#).
- [78] A. Chaudhuri, N. Khan, B. Mukhopadhyaya, and S. Rakshit, “Dark matter candidate in an extended type III seesaw scenario,” *Phys. Rev. D* **91** (2015) 055024, [arXiv:1501.05885 \[hep-ph\]](#).
- [79] K. R. Dienes and B. Thomas, “Dynamical Dark Matter: I. Theoretical Overview,” *Phys. Rev. D* **85** (2012) 083523, [arXiv:1106.4546 \[hep-ph\]](#).
- [80] D. Borah, B. Karmakar, and D. Nanda, “Common Origin of Dirac Neutrino Mass and Freeze-in Massive Particle Dark Matter,” *JCAP* **07** (2018) 039, [arXiv:1805.11115 \[hep-ph\]](#).
- [81] A. Biswas and A. Gupta, “Freeze-in Production of Sterile Neutrino Dark Matter in $U(1)_{B-L}$ Model,” *JCAP* **09** (2016) 044, [arXiv:1607.01469 \[hep-ph\]](#). [Addendum: *JCAP* **05**, A01 (2017)].
- [82] F. Elahi, C. Kolda, and J. Unwin, “UltraViolet Freeze-in,” *JHEP* **03** (2015) 048, [arXiv:1410.6157 \[hep-ph\]](#).
- [83] **Muon g-2** Collaboration, B. Abi *et al.*, “Measurement of the Positive Muon Anomalous Magnetic Moment to 0.46 ppm,” *Phys. Rev. Lett.* **126** (2021) 141801, [arXiv:2104.03281 \[hep-ex\]](#).
- [84] **Muon g-2** Collaboration, G. W. Bennett *et al.*, “Final Report of the Muon E821 Anomalous Magnetic Moment Measurement at BNL,” *Phys. Rev. D* **73** (2006) 072003, [arXiv:hep-ex/0602035](#).
- [85] R. H. Parker, C. Yu, W. Zhong, B. Estey, and H. Müller, “Measurement of the fine-structure constant as a test of the Standard Model,” *Science* **360** (2018) 191, [arXiv:1812.04130 \[physics.atom-ph\]](#).
- [86] J. Aebischer, W. Dekens, E. E. Jenkins, A. V. Manohar, D. Sengupta, and P. Stoffer, “Effective field theory interpretation of lepton magnetic and electric dipole moments,” [arXiv:2102.08954](#)

- [hep-ph].
- [87] T. Abe, R. Sato, and K. Yagyu, “Muon specific two-Higgs-doublet model,” *JHEP* **07** (2017) 012, [arXiv:1705.01469](#) [hep-ph].
- [88] E. J. Chun and J. Kim, “Leptonic Precision Test of Leptophilic Two-Higgs-Doublet Model,” *JHEP* **07** (2016) 110, [arXiv:1605.06298](#) [hep-ph].
- [89] S. Baek, N. Deshpande, X. He, and P. Ko, “Muon anomalous $g-2$ and gauged $L(\muon) - L(\tau)$ models,” *Phys. Rev. D* **64** (2001) 055006, [arXiv:hep-ph/0104141](#).
- [90] M. Endo, K. Hamaguchi, and G. Mishima, “Constraints on Hidden Photon Models from Electron $g-2$ and Hydrogen Spectroscopy,” *Phys. Rev. D* **86** (2012) 095029, [arXiv:1209.2558](#) [hep-ph].
- [91] Y. Abe, T. Toma, and K. Tsumura, “A μ - τ -philic scalar doublet under Z_n flavor symmetry,” *JHEP* **06** (2019) 142, [arXiv:1904.10908](#) [hep-ph].
- [92] S. Jana, P. K. Vishnu, W. Rodejohann, and S. Saad, “Dark matter assisted lepton anomalous magnetic moments and neutrino masses,” *Phys. Rev. D* **102** no. 7, (2020) 075003, [arXiv:2008.02377](#) [hep-ph].
- [93] D. Sabatta, A. S. Cornell, A. Goyal, M. Kumar, B. Mellado, and X. Ruan, “Connecting muon anomalous magnetic moment and multi-lepton anomalies at LHC,” *Chin. Phys. C* **44** no. 6, (2020) 063103, [arXiv:1909.03969](#) [hep-ph].
- [94] S. von Buddenbrock, N. Chakrabarty, A. S. Cornell, D. Kar, M. Kumar, T. Mandal, B. Mellado, B. Mukhopadhyaya, R. G. Reed, and X. Ruan, “Phenomenological signatures of additional scalar bosons at the LHC,” *Eur. Phys. J. C* **76** no. 10, (2016) 580, [arXiv:1606.01674](#) [hep-ph].
- [95] L. Calibbi, R. Ziegler, and J. Zupan, “Minimal models for dark matter and the muon $g-2$ anomaly,” *JHEP* **07** (2018) 046, [arXiv:1804.00009](#) [hep-ph].
- [96] N. Chen, B. Wang, and C.-Y. Yao, “The collider tests of a leptophilic scalar for the anomalous magnetic moments,” [arXiv:2102.05619](#) [hep-ph].
- [97] W. Yin, “Radiative lepton mass and muon $g - 2$ with suppressed lepton flavor and CP violations,” [arXiv:2103.14234](#) [hep-ph].
- [98] E. J. Chun and T. Mondal, “Searching for a Light Higgs Boson via the Yukawa Process at Lepton Colliders,” *Phys. Lett. B* **802** (2020) 135190, [arXiv:1909.09515](#) [hep-ph].
- [99] K. S. Babu, “TASI Lectures on Flavor Physics,” in *Proceedings of Theoretical Advanced Study Institute in Elementary Particle Physics on The dawn of the LHC era (TASI 2008): Boulder, USA, June 2-27, 2008*, pp. 49–123. 2010. [arXiv:0910.2948](#) [hep-ph].
- [100] E. Ma and D. Suematsu, “Fermion Triplet Dark Matter and Radiative Neutrino Mass,” *Mod. Phys. Lett. A* **24** (2009) 583–589, [arXiv:0809.0942](#) [hep-ph].
- [101] T. Araki, C. Q. Geng, and K. I. Nagao, “Dark Matter in Inert Triplet Models,” *Phys. Rev. D* **83** (2011) 075014, [arXiv:1102.4906](#) [hep-ph].

- [102] A. Das, T. Nomura, H. Okada, and S. Roy, “Generation of a radiative neutrino mass in the linear seesaw framework, charged lepton flavor violation, and dark matter,” *Phys. Rev. D* **96** no. 7, (2017) 075001, [arXiv:1704.02078 \[hep-ph\]](#).
- [103] E. Ma, “Verifiable radiative seesaw mechanism of neutrino mass and dark matter,” *Phys. Rev. D* **73** (2006) 077301, [arXiv:hep-ph/0601225 \[hep-ph\]](#).
- [104] S. Bhattacharya, N. Sahoo, and N. Sahu, “Singlet-Doublet Fermionic Dark Matter, Neutrino Mass and Collider Signatures,” *Phys. Rev. D* **96** no. 3, (2017) 035010, [arXiv:1704.03417 \[hep-ph\]](#).
- [105] P. Das, M. K. Das, and N. Khan, “A new feasible dark matter region in the singlet scalar scotogenic model,” *Nucl. Phys. B* **964** (2021) 115307, [arXiv:2001.04070 \[hep-ph\]](#).
- [106] T. Cohen, J. Kearney, A. Pierce, and D. Tucker-Smith, “Singlet-Doublet Dark Matter,” *Phys. Rev. D* **85** (2012) 075003, [arXiv:1109.2604 \[hep-ph\]](#).
- [107] K. Griest and M. Kamionkowski, “Unitarity Limits on the Mass and Radius of Dark Matter Particles,” *Phys. Rev. Lett.* **64** (1990) 615.
- [108] K. Kowalska and E. M. Sessolo, “Expectations for the muon $g-2$ in simplified models with dark matter,” *JHEP* **09** (2017) 112, [arXiv:1707.00753 \[hep-ph\]](#).
- [109] K. Kowalska and E. M. Sessolo, “Minimal models for $g - 2$ and dark matter confront asymptotic safety,” [arXiv:2012.15200 \[hep-ph\]](#).
- [110] J. Kawamura, S. Okawa, and Y. Omura, “Current status and muon $g - 2$ explanation of lepton portal dark matter,” *JHEP* **08** (2020) 042, [arXiv:2002.12534 \[hep-ph\]](#).
- [111] M. J. Baker, P. Cox, and R. R. Volkas, “Radiative muon mass models and $(g - 2)_\mu$,” *JHEP* **05** (2021) 174, [arXiv:2103.13401 \[hep-ph\]](#).
- [112] P. B. Pal, *An introductory course of particle physics*. Taylor & Francis, 2014.
- [113] F. Pisano and A. T. Tran, “Anomaly cancellation in a class of chiral flavor gauge models,” in *14th Brazilian Meeting on Particles and Fields*. 7, 1993.
- [114] **MEG II** Collaboration, A. M. Baldini *et al.*, “The design of the MEG II experiment,” *Eur. Phys. J. C* **78** no. 5, (2018) 380, [arXiv:1801.04688 \[physics.ins-det\]](#).
- [115] W. Chao, “The Muon Magnetic Moment in the TeV Scale Seesaw Models,” [arXiv:0806.0889 \[hep-ph\]](#).
- [116] C.-H. Chen and T. Nomura, “Influence of an inert charged Higgs boson on the muon $g - 2$ and radiative neutrino masses in a scotogenic model,” *Phys. Rev. D* **100** no. 1, (2019) 015024, [arXiv:1903.03380 \[hep-ph\]](#).
- [117] M. Bauer and T. Plehn, *Yet Another Introduction to Dark Matter: The Particle Physics Approach*, vol. 959 of *Lecture Notes in Physics*. Springer, 2019. [arXiv:1705.01987 \[hep-ph\]](#).
- [118] P. Gondolo and G. Gelmini, “Cosmic abundances of stable particles: Improved analysis,” *Nucl. Phys. B* **360** (1991) 145–179.

- [119] A. Alloul, N. D. Christensen, C. Degrande, C. Duhr, and B. Fuks, “FeynRules 2.0 - A complete toolbox for tree-level phenomenology,” *Comput. Phys. Commun.* **185** (2014) 2250–2300, [arXiv:1310.1921 \[hep-ph\]](#).
- [120] G. Bélanger, F. Boudjema, A. Goudelis, A. Pukhov, and B. Zaldivar, “micrOMEGAs5.0 : Freeze-in,” *Comput. Phys. Commun.* **231** (2018) 173–186, [arXiv:1801.03509 \[hep-ph\]](#).
- [121] F. Staub, “Exploring new models in all detail with SARAH,” *Adv. High Energy Phys.* **2015** (2015) 840780, [arXiv:1503.04200 \[hep-ph\]](#).
- [122] W. Porod and F. Staub, “SPHeno 3.1: Extensions including flavour, CP-phases and models beyond the MSSM,” *Comput. Phys. Commun.* **183** (2012) 2458–2469, [arXiv:1104.1573 \[hep-ph\]](#).
- [123] K. Griest and D. Seckel, “Three exceptions in the calculation of relic abundances,” *Phys. Rev.* **D43** (1991) 3191–3203.
- [124] N. Arkani-Hamed, D. P. Finkbeiner, T. R. Slatyer, and N. Weiner, “A Theory of Dark Matter,” *Phys. Rev.* **D79** (2009) 015014, [arXiv:0810.0713 \[hep-ph\]](#).
- [125] C. E. Yaguna, “The Singlet Scalar as FIMP Dark Matter,” *JHEP* **08** (2011) 060, [arXiv:1105.1654 \[hep-ph\]](#).
- [126] N. Bernal, M. Heikinheimo, T. Tenkanen, K. Tuominen, and V. Vaskonen, “The Dawn of FIMP Dark Matter: A Review of Models and Constraints,” *Int. J. Mod. Phys.* **A32** no. 27, (2017) 1730023, [arXiv:1706.07442 \[hep-ph\]](#).
- [127] G. Choi, T. T. Yanagida, and N. Yokozaki, “Feebly interacting $U(1)_{B-L}$ gauge boson warm dark matter and XENON1T anomaly,” *Phys. Lett. B* **810** (2020) 135836, [arXiv:2007.04278 \[hep-ph\]](#).
- [128] **Planck** Collaboration, N. Aghanim *et al.*, “Planck 2018 results. VI. Cosmological parameters,” *Astron. Astrophys.* **641** (2020) A6, [arXiv:1807.06209 \[astro-ph.CO\]](#). [Erratum: *Astron. Astrophys.* 652, C4 (2021)].
- [129] P. S. Bhupal Dev, A. Mazumdar, and S. Qutub, “Constraining Non-thermal and Thermal properties of Dark Matter,” *Front. in Phys.* **2** (2014) 26, [arXiv:1311.5297 \[hep-ph\]](#).
- [130] D. Gruber, J. Matteson, L. Peterson, and G. Jung, “The spectrum of diffuse cosmic hard x-rays measured with heao-1,” *Astrophys. J.* **520** (1999) 124, [arXiv:astro-ph/9903492](#).
- [131] L. Bouchet, E. Jourdain, J. Roques, A. Strong, R. Diehl, F. Lebrun, and R. Terrier, “INTEGRAL SPI All-Sky View in Soft Gamma Rays: Study of Point Source and Galactic Diffuse Emissions,” *Astrophys. J.* **679** (2008) 1315, [arXiv:0801.2086 \[astro-ph\]](#).
- [132] K. S. C., *Ph. D. Thesis*. PhD thesis, University of New Hampshire, USA, 1998.
- [133] A. W. Strong, I. V. Moskalenko, and O. Reimer, “Diffuse galactic continuum gamma rays. A Model compatible with EGRET data and cosmic-ray measurements,” *Astrophys. J.* **613** (2004) 962–976, [arXiv:astro-ph/0406254](#).

- [134] R. Essig, E. Kuflik, S. D. McDermott, T. Volansky, and K. M. Zurek, “Constraining Light Dark Matter with Diffuse X-Ray and Gamma-Ray Observations,” *JHEP* **11** (2013) 193, [arXiv:1309.4091](#) [[hep-ph](#)].
- [135] J. F. Navarro, C. S. Frenk, and S. D. White, “A Universal density profile from hierarchical clustering,” *Astrophys. J.* **490** (1997) 493–508, [arXiv:astro-ph/9611107](#).
- [136] J. M. No, P. Tunney, and B. Zaldivar, “Probing Dark Matter freeze-in with long-lived particle signatures: MATHUSLA, HL-LHC and FCC-hh,” *JHEP* **03** (2020) 022, [arXiv:1908.11387](#) [[hep-ph](#)].